

https://dspace.org/

Spatiotemporal analysis of weatherrelated fire danger associated with climate change in the Zagros Mountanis Iran

G Roshan; A Ghanghermeh; M Eshaghi; R Sarli; Stefan Grab

https://hdl.handle.net/10539/47608
WOS

Downloaded from a DSpace repository. https://dspace.org/

Stochastic Environmental Research and Risk Assessment (2025) 39:55–80
https://doi.org/10.1007/s00477-024-02850-9

ORIGINAL PAPER

Spatiotemporal analysis of weather-related fire danger associated with climate change in the Zagros Mountains, Iran

Gholamreza Roshan[1] · Abdolazim Ghanghermeh[1] · Mohammad Amin Eshaghi[2] · Reza Sarli[3] · Stefan W. Grab[4]

Accepted: 23 October 2024 / Published online: 16 November 2024
© The Author(s), under exclusive licence to Springer-Verlag GmbH Germany, part of Springer Nature 2024

Abstract
This study uses the Fire Weather Index (FWI) from the Canadian Wildfire Hazard Rating System (CFFDRS) to assess the danger of future wildfires in the Zagros Mountains under climate change. We use CanESM5 model data for the SSP245 and SSP585 scenarios to estimate FWI changes in the past (1960–2020), near future (2031 – 2017), and distant future (2061–2090). Statistical analysis at the 95% confidence level verifies significant differences in FWI values, especially in the Northwest. We explore spatial and temporal trends using Emerging Hot Spot Analysis (EHSA). The results show that cold spots are decreasing, and warm spots are increasing over time. The results of this study highlight the continuing dangers of wildfires in the region. The study underscores the significance of implementing preventive fire management strategies that consider the dynamic nature of weather patterns.

Keywords Geospatial data · Emerging hot spots · Fire weather index · Forests · Shared socioeconomic pathways (SSPs)

1 Introduction

Global climate change is considered one of the most pressing environmental, societal and political challenges of our time (e.g., Bulkeley and Newell 2010; Giddens 2015; Jansson and Hofmockel 2020). In the context of recent global warming, there have been increased hazards associated with wildfires in natural ecosystems (Kussul et al. 2023; Gajendiran et al., 2024; Vigna et al., 2023). The rapid decimation of global forests continues unabated, driven by a combination of intensive agriculture and climate warming associated rampant wildfires (Jones et al. 2022). Since the turn of the century, forest coverage has been halved due to human-induced deforestation (Barnes et al. 2024; Ahmadi et al. 2024). Rapidly rising global temperatures and drought have compounded this problem through making many remaining forests vulnerable to disease and mortality (Allen et al., 2010).

In the field of wildland fire management, "fire danger" is defined as the environmental conditions that affect the likelihood of a fire igniting and spreading. This includes factors such as atmospheric conditions (temperature, humidity, and wind), as well as fuel moisture content. Tools like the Fire Danger Rating System (FDRS) are commonly used to evaluate these conditions and predict fire behavior (Preisler et al. 2005; Vadrevu 2021). On the other hand, "fire risk" encompasses both the probability of a fire starting and the potential consequences of that fire. It considers not only environmental variables but also human activities, land use patterns, and the susceptibility of communities and ecosystems to fire impacts. Therefore, while fire danger provides insight into immediate conditions that may lead to fire, fire risk offers a comprehensive view of the overall threat posed by wildfires (Miller and Ager, 2012; Ascoli et al. 2023).

Forest fires are caused by a wide range of factors, including both natural phenomena and human activities (Bedia

✉ Gholamreza Roshan
ghr.roshan@gu.ac.ir

✉ Abdolazim Ghanghermeh
a.ghanghermeh@gu.ac.ir

[1] Department of Geography, Golestan University, Gorgan 49138-15759, Iran

[2] Forestry Department, Faculty of Forest Sciences, Gorgan University of Agricultural Sciences and Natural Resources, Gorgan, Iran

[3] Department of Forest Resources Management, Faculty of Forestry, University of Agriculture in Krakow, AL. 29 Listopada46, Kraków 31-425, Poland

[4] School of Geography, Archaeology and Environmental Studies, University of the Witwatersrand, Johannesburg, South Africa

et al. 2015; Rodrigues et al., 2018). Natural causes may include lightning strikes, volcanic eruptions, and spontaneous combustion. Conversely, human-induced factors involve unregulated agricultural practices, alterations in land use, deliberate arson, and negligence. Vulnerability to fires is exacerbated by climate warming, which amplifies the frequency and intensity of wildfires (Zidda et al., 2023). From an ecological perspective, forest fires yield far-reaching repercussions such as ravaging habitats and jeopardizing plant and animal species. Additionally, forest fires disrupt vital ecological mechanisms, including nutrient cycling, and reshape patterns of succession and regeneration (Chungu et al. 2019; Rustowska, 2022). Furthermore, forest fires heighten susceptibility to invasive species, thus compounding their ecological fragility (Nikolopoulos et al. 2018; Mansourihanis et al. 2024b). Soil degradation is an additional consequence of forest fires through nutrient depletion, diminished fertility and reducing soil shear strength (Campos et al. 2016; Abney et al. 2017).

Numerous studies have investigated the effects of climate change on forest fires, some of which we summarize. Recently, Krikken et al. (2021) analyzed the relationship between climate change and the 2018 forest fires in Sweden using the Canadian Fire Weather Index. While short-term data indicate a slight decrease in fire risk, climate models forecast a significant increased fire risk under a 2 °C warming scenario, primarily driven by rising temperatures and regional changes in precipitation. It has also been established through the FWI that the impact of climate change on wildfire risk has substantially increased over the period 1979–2019, particularly in regions such as the Mediterranean and the Pacific United States Jones et al. 2022). However, the influence of the FWI has been regionally variable, with human activity and fuel availability playing more significant roles in savannahs. FWI using climate scenarios RCP 4.5 and RCP 8.5 have revealed a notable increase in fire risk in southern France, including a doubling of high and very high FWI days in areas such as Provence-Alpes-Côte d'Azur and Corsica, accompanied by heightened Initial and Seasonal Spread Indices (Varela et al., 2019). A subsequent study utilized the FWI and EURO-CORDEX climate models to similarly demonstrate that wildfires in Mediterranean France will likely increase, particularly under RCP 4.5 and RCP 8.5 scenarios (Fargeon et al. 2020). Their findings indicated a doubling of high fire danger days attributed to rising temperatures, reduced humidity, and alterations in wind patterns, underscoring the necessity for improved wildfire management strategies. Such patterns extend to northern Spain and northwestern Portugal, for which increased fire risk under climate scenarios RCP 2.6, RCP 4.5, and RCP 8.5 have been projected, including also a lengthening of the fire season (Bento et al. 2023). Similar findings have emerged from studies in eastern Europe where a rising trend in fire danger with elevated FWI values has been established for southeastern regions of Belarus and Ukraine over the period 1990–2020, driven by climate change (Semenova et al., 2022). The outcomes of these studies highlight the importance of establishing early warning systems for future fire prevention and enhanced capacity for fire management.

In Iran, the fragile forest and grassland ecosystems are also under increasing threat from wildfires (Eskandari and Chuvieco 2015). These fires have become synonymous with the yearly environmental challenges that Iran faces, amplified by a rapidly warming and drying climate (Jahdi et al. 2020). According to climate projections, Iran is expected to experience an increase in the frequency and intensity of summer heatwaves (Modarres, et al., 2018; Masaeli et al. 2023), which increases the danger of fire occurrence and intensity (Sousa-Silva et al., 2018). As a low forest cover nation, the repercussions of such wildfires are profound and multifaceted (Jahdi et al. 2023). Moreover, the aftermath of such fires is characterized by a cascade of secondary consequences such as diminished air quality and associated health hazards, destabilized regolith and associated soil loss and mass movement hazards (e.g., landslides), and infrastructural losses (Grant and Runkle, 2022; Di Napoli et al. 2020). Given that forest fires in Iran have notable impacts on the environment, local societies and the economy (Ghorbanzadeh et al. 2019), it is appropriate and important to better ascertain spatial and temporal patterns of such fires (Matin et al. 2017).

Given the significant environmental impacts of forest fires, a valuable initiative is to record, monitor and forecast forest fires for given regions (Tian et al., 2022; Mishra et al., 2024; Mansourihanis et al. 2023). Such work would entail fire danger rating, fire behavior prediction, and fire spread simulation modelling. The prediction of forest fires has been the subject of extensive study. Notable examples include the Canadian Forest Fire Danger Rating System (CFFDRS), the U.S. Forest Service National Fire Danger Rating System (NFDRS), and the McArthur Forest Fire Danger Index (FFDI) (Di Giuseppe et al. 2016). Numerous fire danger indices have been developed to establish fire danger (Bett et al. 2020). While many fire danger indices are designed for specific geographic regions, others, such as the Fire Weather Index (FWI), offer versatility in assessing present and future fire danger levels across various scales, ranging from local to global contexts (Fujioka et al. 2008; Grillakis et al. 2022).

The Fire Weather Index (FWI), pioneered by Van Wagner in 1974, stands out for its superior efficiency compared to other forest fire indices (Schunk et al. 2016; Tremblay et al., 2018; Mansourihanis et al. 2024a). The Fire Weather Index (FWI) assesses the impact of meteorological factors on forest fuel and fire occurrences by offering a relative numerical

assessment of fire danger across a specified area (Stocks et al., 1989). Initially tailored for Canadian pine stands, the Fire Weather Index (FWI) has been widely embraced across diverse forest environments owing to its adaptability. Additionally, it has received broad acceptance from numerous fire and land management agencies, which utilize it for issuing fire alerts and deploying field resources. However, it should be noted that the FWI system primarily provides a qualitative overview of projected fire regimes. Nonetheless, numerous studies have confirmed a robust association between FWI codes/indices and both fire incidence and behavior (e.g., Dimitrakopoulos et al., 2011; Papagiannaki et al. 2020).

The primary aim of this study is to explore whether recent climatic changes have influenced weather-related fire danger in the Zagros Mountains over the past decades, and to project future fire danger. To achieve this, we analyze the temporal variation of fire danger across different spatio-meteorological conditions, as indicated by the FWI. The study compares future periods (2031–2060 and 2061–2090) with a reference period (1960–2020). We hypothesize that climatic changes significantly impact fire danger patterns, which can be detected using Emerging Hot Spot Analysis. This method, applied at a national scale in Iran, is innovative and has rarely been used internationally for assessing spatial-temporal fire danger variability.

2 Study region

The Zagros Mountain range, extending from northwestern Iran, southeastward and parallel to the Persian Gulf (Fig. 1), is not only a prominent physical landmark, but also an ecological and climatic keystone of the region. Spanning over 1,500 km in length and varying in width from 200 to 400 km, the Zagros is characterized by its rugged terrain, high peaks, and extensive forested areas (Zafarani and Soghrat 2012). This mountain range plays a crucial role in shaping the climate of the surrounding areas, influencing precipitation patterns, and serving as a critical water source for both human populations and biodiversity (Noroozi et al. 2020). The Zagros mountains are home to rich and diverse ecosystems, including expansive forests of oak, pistachio, and almond trees, which are integral to the environmental and economic

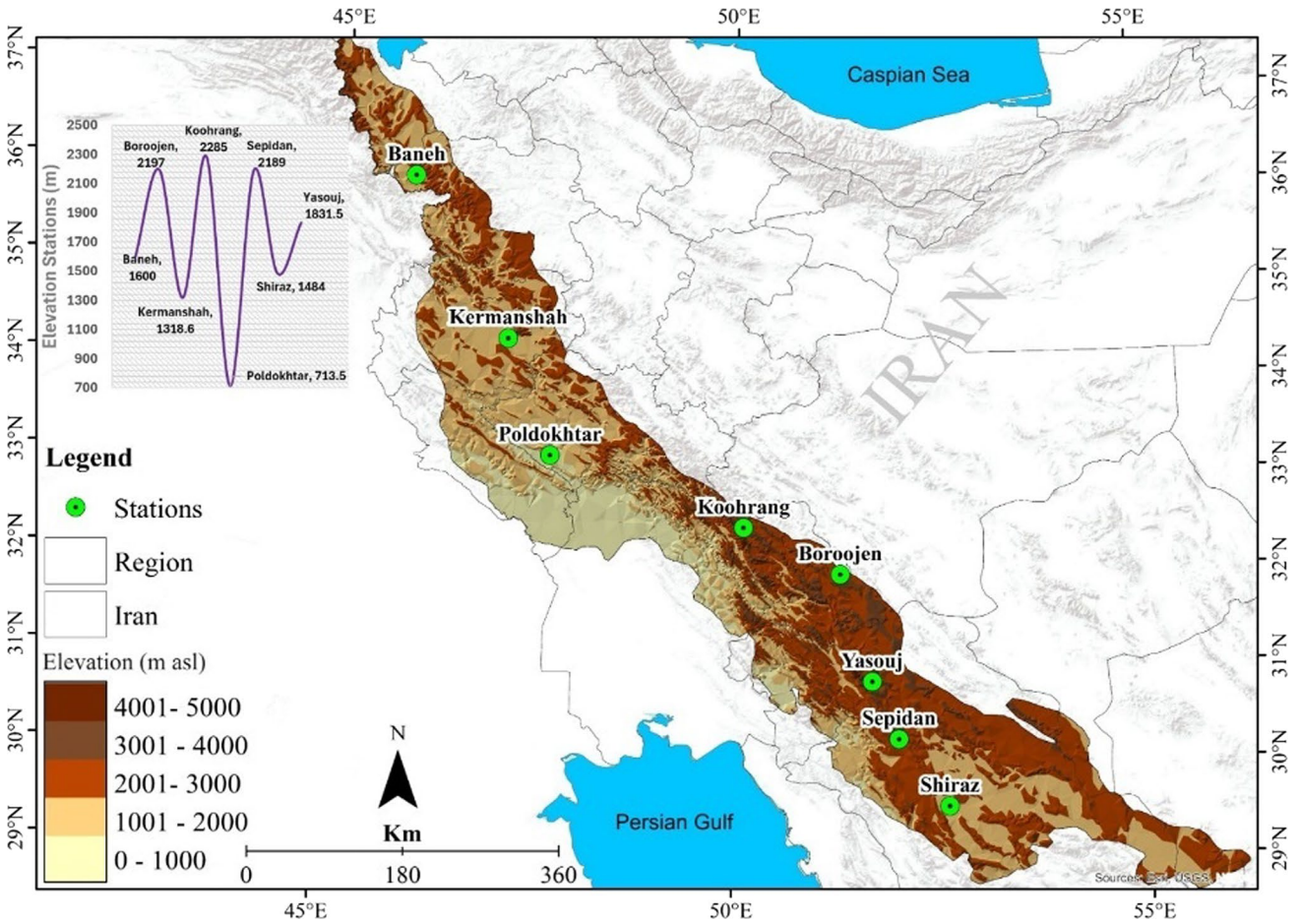


Fig. 1 The Zagros Mountain study region

health of the region. These forests not only act as significant carbon sinks, aiding in the fight against climate change, but also provide habitat for a variety of wildlife species, making the Zagros a vital area for conservation efforts. The region's diverse climates, from the cold, snowy northern reaches to the warmer, semi-arid zones in the south, contribute to the wide range of agricultural products and traditional lifestyles found along its expanse (Noroozi et al. 2020). In the context of forest fire danger, the Zagros Mountain range presents a unique set of challenges and conditions. The variability in elevation, climate, and vegetation types across the range affects fire behavior and danger, making the study of fire weather indices (particularly the FWI) essential for understanding and mitigating fire dangers in these forests. The combination of natural beauty, ecological significance, and the threat posed by forest fires, makes the Zagros mountains an important and timely focus for research aimed at preserving these landscapes for future generations (Ghaedi et al. 2020).

3 Data and methodology

3.1 FWI data

The FWI represents the final component within the FWI System, derived from the integration of three primary sub-indices assessing fuel moisture (Fine Fuel Moisture Code, Duff Moisture Code, and Drought Code), along with two intermediate sub-indices evaluating spread rate (Initial Spread Index) and fuel accumulation (Buildup Index) (Varela et al., 2019; Bento et al. 2023) (Fig. 2). In our study, we solely focus on FWI, as it amalgamates the impacts of all FWI System components while also offering a quantitative assessment of fire intensity. Thus, it serves as a comprehensive index for gauging fire danger.

The NEX-GDDP-CMIP6 dataset comprises global downscaled climate scenarios obtained from General Circulation Model (GCM) runs conducted within the framework of the Coupled Model Intercomparison Project Phase 6 (CMIP6). These scenarios encompass two of the four "Tier 1" greenhouse gas emissions scenarios, known as Shared Socioeconomic Pathways (SSPs). The CMIP6 GCM runs were developed to support the Sixth Assessment Report of the Intergovernmental Panel on Climate Change (IPCC AR6). This dataset includes downscaled projections derived from ScenarioMIP model runs, with daily scenarios disseminated through the Earth System Grid Federation. The Earth Engine public data platform facilitates the extraction and utilization of these data. Climatic data for FWI computation were obtained from Earth Engine's public data platform. Despite FWI indices typically being calculated at noon, Earth Engine only provides daily values of the necessary variables.

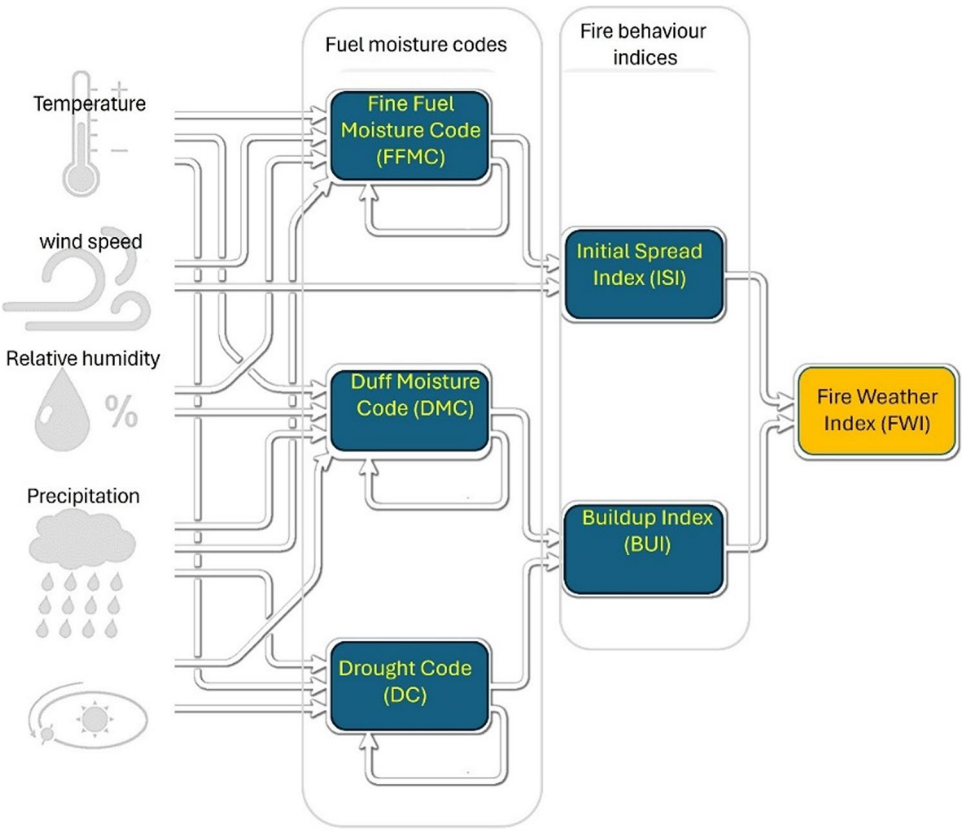


Fig. 2 Structure of the Canadian Forest fire weather index system (after De Groot 1987; de Rigo 2016)

Following methodologies outlined in previous studies (Moriondo et al. 2006; Carvalho et al. 2009; Giannakopoulos et al. 2009; Bento et al. 2023), we computed FWI components based on daily mean 2-m temperature (°C), relative humidity, 10-m wind speed, and daily accumulated precipitation. Consequently, FWI values were estimated daily for each grid-point over historical and future periods, corresponding to two different Shared Socioeconomic Pathways (SSPs). Fire danger classes in this study were determined based on the classification provided in Table 1 (Júnior et al. 2022).

The research period spans from 1960 to 2020 for the historical period, as well as the near-future (2031–2060) and distant-future (2061–2090) periods. All data, both historical and future, were derived from the CanESM5 model for two scenarios, SSP245 and SSP585, with spatial dimensions of 0.25° * 0.25°. To validate the CanESM5 model data, observational data from eight meteorological stations, distributed throughout the region, were utilized (Fig. 1). In addition to station observation data, ECMWF and TRMM satellite databases were also employed for CanESM5 model data validation, for which results are presented in Table 5.

3.2 The Mann–Kendall technique

The Mann-Kendall technique was employed for both temporal and spatial analyses to assess the trend of changes in the FWI in the Zagros Mountain region. Additionally, the hotspot analysis function was utilized to delineate intensity anomaly zones of the FWI. This method involves calculating the difference between each observation and all other observations to obtain the parameter S. For a random sample comprising n observations, the estimator S can be computed using the following equation (Roshan et al., 2016; Zahraei et al., 2019):

$$S = \sum_{k=1}^{n-1} \sum_{j=k+1}^{n} \mathrm{sgn}\left(x_j - x_k\right) \tag{1}$$

Where n is the total number of series observations, x_j and x_k indicate the j_{th} and k_{th} data points, respectively. The "sgn" function may alternatively be computed using the formula below:

$$sgn\left(x_j - x_k\right) = \begin{cases} +1 & for\ \left(x_j - x_k\right) > 0 \\ 0 & for\ \left(x_j - x_k\right) = 0 \\ -1 & for\ \left(x_j - x_k\right) < 0 \end{cases} \tag{2}$$

One of the following equations is then used to obtain the variance of S:

$$\mathrm{Var}\,(S) = \frac{n\,(n-1)\,(2n+5) - \sum_{i=1}^{m} t\,(t-1)\,(2t+5)}{18} \qquad \text{for } n > 1 \tag{3}$$

$$\mathrm{Var}\,(S) = \frac{n\,(n-1)\,(2n+5) - (n2+5)}{18} \qquad \text{for } n < 10$$

Where n and m represent the number of sequences that include at least one duplicate data value. The frequency of similar data in a sequence is denoted by t. Finally, one of the following relations is used to calculate the Z statistic:

$$Z = \frac{S-1}{\sqrt{\mathrm{Var}\,(S)}} \qquad \text{for } S > 0$$

$$\mathbf{Z = 0} \qquad \mathbf{for\ S = 0} \tag{4}$$

$$Z = \frac{S+1}{\sqrt{\mathrm{Var}\,(S)}} \qquad \text{for } S < 0$$

In the case of a two-tailed trend test, the following criteria must be satisfied to accept the null hypothesis:

$$|Z| < Z_{a/2} \tag{5}$$

where *a* is the significance level that is considered for the test and *Za* is the standard normal distribution statistic at the significance level of *a*, which becomes $\frac{a}{2}$ because of the two domains of the test.

The FWI anomaly was subsequently estimated utilizing the Getis-Ord Gi statistic and is determined as follows (Carpio-Pinedo et al. 2022):

$$G_i^* = \frac{\sum_{j=1}^{n} w_{i,j} x_j - \bar{X} \sum_{j=1}^{n} w_{i,j}}{S\sqrt{\frac{\left[n\sum_{j=1}^{n} w^2_{i,j} - \left(\sum_{j=1}^{n} w_{i,j}\right)^2\right]}{n-1}}} \tag{6}$$

In this formula, Xj is the attribute value for complication j, Wij is the spatial weight between complications i and j, and n is equal to the total number of complications.

$$\overline{X} = \frac{\sum_{j=i}^{n} x_j}{n} \qquad S = \sqrt{\frac{\sum_{j=1}^{n} x_j^2}{n} - \left(\overline{X}\right)^2} \tag{7}$$

FWI class	Danger class
<5.2	Very low
5.2 - 11.2	Low
11.2 - 21.3	Moderate
21.3 - 38.0	High
38.0 - 50	Very high
>=50.0	Extreme

Table 1 FWI value categorization

The $G*i$ statistic (z-score) output represents the statistical significance of clustering for a specified distance (ESRI, 2018). The z-score was then compared with a range of values entailing seven confidence levels: -0.01 (values < -2.58); -0.05 (values ranging from − 2.58 to -1.96); -0.1 (values ranging from − 1.96 to -1.65); 0 (values ranging from − 1.65 to1.65); 0.1 (values ranging from 1.65 to 1.96); 0.05 (values ranging from 1.96 to 2.58); and 0.01 (values > 2.58).

We subsequently undertook emerging hotspot analysis (EHA) using ArcGIS Pro software (ESRI, 2023) to elucidate spatiotemporal fluctuations in emergency calls during the study period. EHA is a novel method integrated into GIS-based analyses, and its application in spatiotemporal analysis is widely used (e.g., Rabiei-Dastjerdi and McArdle 2020; Reddy et al., 2020; Hart 2021; Salehi Mava et al. 2022; Morckel and Durst 2021; Khosravi et al. 2024). These data are utilized to analyze different zones based on the frequency of EHSA occurrences in various metropolitan areas over the 23-year period. Using ArcGIS Pro 3.1 software, the categories outlined in Table 2 were utilized for this assessment.

3.3 Remote sensing datasets and LULC maps

The production of accurate LULC maps, through remote sensing, is the first component of studies establishing spatio-temporal characteristics of deforestation (Nasiri et al., 2022b). Based on our research objectives and methodology, we used the capabilities of the Google Earth Engine cloud computing platform to process multisensor Landsat data. As a primary step in LULC mapping, a multitemporal reference dataset, including training and validation samples, was generated based on in situ recording using the Global Positioning System and the visual interpretation of aerial and very-high-resolution (VHR) Google Earth images. Field surveys were performed in the summer of 2020 to collect precise samples, which were grouped in classes with a high level of spectral similarity (Table 3). For the other time points, these samples were overlaid with the abovementioned VHR images, and a revision process undertaken. We conducted a structured process to evaluate land use maps in the years 1992, 2000, and 2010. This method included the visual interpretation of ultrafine Google Earth images as complementary techniques. For each time point (1992, 2000, 2010 and 2020), a total of 911 samples representing six LULC classes were collected as follows: dense and open forests, shrubland, croplands, bare areas, grassland, urban areas, and water bodies. The samples in the reference dataset were randomly divided into training (70%) and testing (30%) subsets. We consequently applied the Kappa coefficients (K_no, K_location, and K_quantity) to measure the concordance between the classified maps and validation samples, enabling a detailed evaluation of all relevant aspects such as overall, spatial, and quantity accuracy.

For the classification features, at each time point, we created an image collection based on all the Landsat images captured during the growing season (from April to September) and calculated pixel-wise spectral–temporal metrics (STMs) based on the resulting image collections. In addition to the spectral bands, common vegetation indices (difference vegetation index [DVI]; normalized DVI [NDVI]; enhanced vegetation index [EVI]) were used to distinguish different vegetation types to perform LULC mapping (Nasiri et al. 2023). Finally, STMs were calculated as the median, standard deviation, minimum, maximum, and percentile (25th, 50th, and 75th) values for all bands and vegetation indices (Table 4). For further analysis, the LULC map was classified into seven distinct classes: urban areas, water bodies, shrubland, grassland, bare areas, dense and open forests, and cropland.

The training samples (Table 3) and STMs (Table 4) were used to train a random forest (RF) model for LULC classification. The RF model, rooted in decision trees, demonstrates exceptional performance in analogous studies owing to its ability to effectively differentiate and map classes sharing similar spectral attributes (Chang et al. 2020; Nasiri et al. 2023). Unlike alternative methods, RF demands less computational time, has fewer parameters to tune, and exhibits adeptness in managing multi-modal data. The effectiveness of the RF model correlates with its hyperparameters employed during training. These parameters can be fine-tuned to enhance the learning process and generate more precise models. In this study, we utilized the GEE-based hyperparameter optimizer to ascertain the optimal LULC value. The alteration in accuracy assessment served as a criterion for determining LULC.

3.4 Change detection, transition potential, and LULC prediction

During the study period, the multitemporal LULC maps were used to identify and track changes. We preferred the Markov Chain (MC) model to the Markov Chain-Cellular Automata (MC-CA) model because of its simplicity, emphasis on transition probabilities, and computational efficiency. The MC model is better suited to studies that emphasize temporal change predictions over complex spatial patterns. It assumes that future land-use changes will primarily follow past trends, making it ideal for making predictions based on historical data. Furthermore, the MC requires less data and has simpler calibration, which is advantageous for studies that focus on temporal analysis. We conducted Markov chain analysis to predict future LULCCs, and then used the predictions as input data to analyze LULC in the coming

Table 2 Spatial and temporal patterns for Emerging Hot Spot Analysis (ESRI, 2023; Ghanghermeh et al. 2024)

Pattern Name	Definition
No Pattern Detected	Does not fall into any of the hot or cold spot patterns defined below.
New Hot Spot	A location that is a statistically significant hot spot for the final time step has never been a statistically significant hot spot.
Consecutive Hot Spot	A location with a single uninterrupted run of statistically significant hot spot bins in the final time-step intervals. The location has never been a statistically significant hot spot before the final hot spot run, and less than 90% of all bins are statistically significant hot spots.
Intensifying Hot Spot	A location that has been a statistically significant hot spot for 90% of the time-step intervals, including the final time step. In addition, the intensity of clustering of high counts in each time step is increasing overall, which is statistically significant.
Persistent Hot Spot	A location that has been a statistically significant hot spot for 90% of the time-step intervals with no discernible trend indicating an increase or decrease in the intensity of clustering over time.
Diminishing Hot Spot	A location that has been a statistically significant hot spot for 90% of the time-step intervals, including the final time step. In addition, the intensity of clustering in each time step is decreasing overall, and that decrease is statistically significant.
Sporadic Hot Spot	A location that is an on-again, then off-again hot spot. Less than 90% of the time-step intervals have been statistically significant hot spots, and none have been statistically significant cold spots.
Oscillating Hot Spot	A statistically significant hot spot for the final time-step interval with a history of also being a significant cold spot during a prior time step. Less than 90% of the time-step intervals have been statistically significant hot spots.
Historical Hot Spot	The most recent period is not hot, but at least 90% of the time-step intervals have been statistically significant hot spots.
New Cold Spot	A location that is a statistically significant cold spot for the final time step and has never been a statistically significant cold spot before.
Consecutive Cold Spot	A location with a single uninterrupted run of statistically significant cold spot bins in the final time-step intervals. The location has never been a statistically significant cold spot before the final cold spot run, and less than 90% of all bins are statistically significant cold spots.
Intensifying Cold Spot	A location that has been a statistically significant cold spot for 90% of the time-step intervals, including the final time step. In addition, the intensity of clustering of low counts in each time step is increasing overall, which is statistically significant.
Persistent Cold Spot	A location that has been a statistically significant cold spot for 90% of the time-step intervals with no discernible trend, indicating an increase or decrease in the intensity of clustering of counts over time.
Diminishing Cold Spot	A location that has been a statistically significant cold spot for 90% of the time-step intervals, including the final time step. In addition, the intensity of clustering of low counts in each time step is decreasing overall, and that decrease is statistically significant.
Sporadic Cold Spot	A location that is an on-again, then off-again cold spot. Less than 90% of the time-step intervals have been statistically significant cold spots, and none have been statistically significant hot spots.
Oscillating Cold Spot	A statistically significant cold spot for the final time-step interval with a history of being a statistically significant hot spot during a prior time step. Less than 90% of the time-step intervals have been statistically significant cold spots.
Historical Cold Spot	The most recent period is not cold, but at least 90% of the time-step intervals have been statistically significant cold spots.

decades. The probability of changing the land cover of a system into a situation at a particular time (t_2) was obtained from information about the same system in the past (t_1) and did not depend on information from times before t_1, as such a transition is a one-time process (Eq. 8). The primary assumption in Markov chain analysis is that future land-use changes are primarily influenced by past trends or patterns in land-use changes. This assumption is rooted in the idea that the transition probabilities between land-use categories remain consistent over time based on historical observations. Essentially, the model assumes that the probabilities of transitioning from one land-use class to another are determined by the historical sequence of changes. This assumption of persistence or dependency on past trends forms the core principle of the Markov Chain model in this study and guides our predictive capability. In the Markov model, the LULCC at t_2 was obtained using its distribution

Table 3 The characteristics of the reference dataset for the year 2020 (pixel size = 30 m)

LULC	Training samples		Validation Samples	
	Samples no	Pixels no	Samples no	Pixels no
Dense and open forests	154	1386	66	594
Shrubland	98	882	42	378
Cropland	98	882	42	378
Bare areas	63	567	27	243
Grassland	84	756	36	324
Water bodies	63	567	27	243
Urban areas	78	697	33	288

Table 4 Details of image collections and features used for LULC mapping

	Sensor	Images no	Features (STMs)	Features no
1992	Landsat-5, TM	9	Median, Standard Deviation, Minimum, Maximum and Percentiles (25th, 50th and 75th)	64
2000	Landsat-5, TM	14		
2010	Landsat-5, TM	20		
2020	Landsat-8, OLI	23		

at t_1 by calculating the transition matrix. The Markov chain is expressed as Eq. 9 (Eastman 2003; Rajitha et al., 2010):

$$\mathrm{vt}_2 = \mathrm{Mvt}_1 \tag{8}$$

In this equation, vt_1 is the land cover vector at t_1, vt_2 is the land cover vector at t_2, and M is the transition probability matrix $m \times m$ for the time interval $\Delta t = t_2 - t_1$.

The probability of transition between two states (Pij) is calculated using Eq. 10.

$$\mathrm{Pij} = \frac{\mathrm{n_{ij}}}{\mathrm{n_i}}, \tag{9}$$

where n_i is.

$$\mathrm{n_i} = \sum {}^{\mathrm{q}}_{\mathrm{j=1}} \mathrm{n_{ij}} \tag{10}$$

Here, n_{ij} is the number of pixels of class i at t_1 that are changed into pixels of class j at t_2 and q is the total number of classes.

The Markov chain had three outputs. The model generated a transition probability matrix and a transition area matrix to show the probability of class changes and the number of pixels that may be converted into pixels of other classes. The model also generated a set of status probability images to indicate the position of each landcover (Pontius 2000; Fan et al., 2008). Various biophysical variables were considered: elevation; slope; aspect; and distance from forests, rangelands, croplands, artificial lands, water bodies, and roads. The elevation, slope, and aspect layers were generated based on the shuttle radar topography mission digital elevation model. The distance between LULC classes was calculated based on the multitemporal LULC maps, and the distance between roads was calculated based on a road map obtained from the National Cartographic Center of Iran. The Artificial Neural Network (ANN) model utilized actual changed pixels from the last time point for both training and testing data (dependent variables). The driving forces mentioned earlier served as explanatory variables (independent variables). This approach led to an iterative model calibration process, where the training data enabled the model to estimate change potential in areas without samples. The model computed training RMSE and tested RMSE errors, enabling accurate monitoring of the calibration process. Lower testing errors during iterations signified effective model training, ensuring its readiness for predictive use. Additionally, setting stopping criteria, including RMS = 0.01 and iterations = 1000, was crucial for successful model calibration.

We used past LULC data (from 1992 to 2020) and associated transfer probability maps to forecast future LULCCs. To assess the accuracy of our simulations, we compared the simulated LULC maps with the classified LULC maps using three agreement metrics, namely, K_{no}, $K_{location}$, and $K_{quantity}$ (Eqs. 11–13). This is because these coefficients are widely accepted and provide a more comprehensive assessment of agreement between the actual and projected maps. Kno measures overall agreement, K_location focuses on spatial precision, and K_quantity estimates the accuracy of projected growth across land cover levels. In addition, we used the Kappa coefficient to account for the number of incorrect pixels in the classification. Overall, the Kappa coefficient provides us with a deeper understanding of the model's performance across the dataset.

$$\mathrm{Kno} = \frac{\mathrm{P_0} - \mathrm{NQNL}}{1 - \mathrm{NQNL}} \tag{11}$$

$$\mathrm{Klocation} = \frac{\mathrm{P_0} - \mathrm{MQNL}}{\mathrm{MQPL} - \mathrm{MQNL}} \tag{12}$$

$$\mathrm{Kquantity} = \frac{\mathrm{P_0} - \mathrm{NQML}}{\mathrm{PQML} - \mathrm{NQML}} \tag{13}$$

The observed correct proportion, denoted as $\mathrm{P_0}$, measures the accuracy of the results. $NQNL$ represents the expected correct proportion in cases without quantity and location information. $MQNL$ indicates the percentage of correct outcomes when there is a moderate ability to specify the

quantity but no ability to specify the location. $MQPL$ represents the percentage of correct outcomes when there is a moderate ability to specify the quantity and a perfect ability to specify the location. $NQML$ indicates the percentage of correct outcomes when there is no ability to specify the quantity and a moderate ability to specify the location (for additional details, see Pontius 2000). Following the accuracy assessment of the simulated LULC maps, we used all observed changes to forecast LULCCs for the years 2030, 2040, 2050, 2060, 2070, 2080 and 2090.

4 Results

4.1 Validation of model data based on observational data

Validation of the CanESM5 model data was conducted using station observation and reanalysis data. Seven sample stations with long and reliable statistical records were selected from the target area, and the validity of these time series was assessed using various statistical methods. It is important to note that while the output of the CanESM5 model has a spatial resolution of 0.25°, observational data are available at a station scale. Therefore, in addition to using observational data, reanalysis data from two ECMWF databases and TRMM satellite output data were utilized, with spatial dimensions of 0.1° and 0.25°, respectively. These databases were only utilized for precipitation (TRMM) and wind (ECMWF), which exhibit greatest spatial variability. For temperature and relative humidity, the same station observation data were utilized. Overall, the validity of CanESM5 data was evaluated for all stations by using observational, ECMWF and TRMM time series data. The outcome demonstrates high validity and confidence levels. However, among the four climate components considered, the wind component of the CanESM5 model had a lower confidence level compared to other variables. For Baneh (p-value = 0.244), Kuhrang (p-value = 0.578) and Poldokhtar (p-value = 0.118) stations, the credibility of the CanESM5 model data, compared to the observational time series, was not statistically significant. However, based on the ECMWF database, the validity of the CanESM5 model data is confirmed. Wind variability is known to be highly dependent on local variations, leading to potentially significant differences between observed values at the station level and those of the CanESM5 model, with a resolution of 0.25 degrees. However, the spatial dimensions of the ECMWF time series used in this study closely match those of the CanESM5 model, thus supporting the validity of the CanESM5 model data, as indicated by the obtained p-value < 0.05 (see Table 5).

4.2 Temporal analysis of intra-annual changes in FWI

Initially, long-term seasonal averages of the FWI index were determined for different seasons of the year, and subsequently, the frequency of the FWI values (> 38) identified for each season. Given that the "very high" and "extreme" classes entail greater danger intensity, the frequency analysis was solely based on FWI values > 38. Essentially, frequencies refer to the average number of days experiencing FWI values > 38 in each season. Seasonal FWI averages increase successively from winter through spring, then autumn and summer (Fig. 2). Based on the overall averages of all scenarios (SSP245 and SSP585) and study periods (reference and future), it is evident that the lowest seasonal average belongs to winter (5.52), followed by spring (16.64), autumn (34.57) and summer (51.62). Findings indicate that for the SSP245 scenario, the seasonal FWI average increased for both the near-future decades (2031–2060) and the distant-future decades (2061–2090), compared to the reference period. Since these changes show a higher rate for the distant-future compared to the near-future, it is projected that the seasonal FWI average for the distant-future will increase by 2.4 in winter, by 1.5 in spring, and by 4.4 and 3.7 for summer and autumn respectively. For SSP585, it is also evident that FWI values have increased in both near- and distant-future periods, with a higher rate observed for the 2061–2090 period. Hence, for the distant future, the FWI average is projected to increase to 2.56, 0.91, 6.33, and 6.03, for winter, spring, summer and autumn respectively, compared to the reference period. In both scenarios, it is evident that the summer season will experience the highest rate of increase in seasonal FWI averages for future decades, while the cold seasons (autumn and winter) will not be exempt from this increase in seasonal FWI averages (Fig. 2).

The percentage of FWI > 38 values was also established for each season, which, considering the entire study period (1960–2090), indicates that only 0.22% of days experienced values exceeding this threshold in winter, 12.56% in spring, 46.97% in autumn, and 84.14% in summer. Both scenarios indicate that except for spring in the SSP585 scenario, which experienced a reduction in frequency by -0.37% and − 0.129% for the near- and distant-futures, respectively, other seasons show increasing frequencies for both scenarios. For the SSP245 scenario, the highest rate of increase in the near future is in summer (4.23%), followed closely by autumn (4.12%). However, for the distant future, the highest rate of increase is in autumn (8.38%), followed by summer (4.68%). For

Table 5 Validation of CanESM5 data based on observation, ECMWF and TRMM data for seven selected stations

Stations	Model	*R*	*R* square	Adjusted *R* square	Durbin-Watson	F	Sig.
Baneh	Obs-Wind	.086[a]	0.007	0.002	1.509	1.366	.244[b]
	ECMWF-Wind	.159[a]	0.025	0.020	0.669	4.712	.031[b]
	Obs-Rain	.473[a]	0.224	0.220	1.370	52.822	.000[b]
	TRMM-Rain	.496[a]	0.246	0.242	1.258	59.632	.000[b]
	Obs-Tem	.971[a]	0.943	0.943	1.560	3054.404	.000[b]
	Obs-Humidity	.875[a]	0.765	0.764	1.340	595.447	.000[b]
Borujen	Obs-wind	.154[a]	0.024	0.019	0.494	4.786	.030[b]
	ECMWF-Wind	.557[a]	0.310	0.306	1.624	88.874	.000[b]
	Obs-Rain	.340[a]	0.116	0.111	1.465	26.387	.000[b]
	TRMM-Rain	.305[a]	0.093	0.088	1.244	20.656	.000[b]
	Obs-Tem	.965[a]	0.931	0.930	1.338	3999.262	.000[b]
	Obs-Humidity	.800[a]	0.640	0.639	1.146	529.196	.000[b]
Kermanshah	Obs-Wind	.215[a]	0.046	0.042	0.698	9.768	.002[b]
	ECMWF-Wind	.001[a]	0.000	-0.005	1.873	0.000	.989[b]
	Obs-Rain	.439[a]	0.193	0.189	1.370	48.204	.000[b]
	TRMM-Rain	.402[a]	0.162	0.158	1.078	38.985	.000[b]
	Obs-Tem	.973[a]	0.947	0.947	1.425	5373.625	.000[b]
	Obs-Humidity	.862[a]	0.744	0.743	1.210	865.166	.000[b]
Kuhrang	Obs-Wind	.039[a]	0.002	-0.003	0.809	0.311	.578[b]
	ECMWF-Wind	.189[a]	0.036	0.031	1.530	7.443	.007[b]
	Obs-Rain	.370[a]	0.137	0.133	1.186	32.015	.000[b]
	TRMM-Rain	.400[a]	0.160	0.156	1.068	38.499	.000[b]
	Obs-Tem	.967[a]	0.936	0.935	1.185	4327.881	.000[b]
	Obs-Humidity	.850[a]	0.723	0.722	1.147	778.320	.000[b]
Poldokhtar	Obs-Wind	.114[a]	0.013	0.008	0.879	2.472	.118[b]
	ECMWF-Wind	.376[a]	0.142	0.137	1.857	31.198	.000[b]
	Obs-Rain	.534[a]	0.285	0.281	1.603	75.639	.000[b]
	TRMM-Rain	.453[a]	0.205	0.201	1.146	48.990	.000[b]
	Obs-Tem	.976[a]	0.953	0.952	1.458	3926.817	.000[b]
	Obs-Humidity	.890[a]	0.791	0.790	1.390	739.023	.000[b]
Sepdan	Obs-Wind	.685[a]	0.470	0.465	1.521	104.558	.000[b]
	ECMWF-Wind	.538[a]	0.290	0.283	1.417	48.081	.000[b]
	Obs-Rain	.418[a]	0.175	0.168	1.277	24.964	.000[b]
	TRMM-Rain	.401[a]	0.161	0.154	1.228	22.665	.000[b]
	Obs-Tem	.966[a]	0.934	0.933	1.352	1658.821	.000[b]
	Obs-Humidity	.783[a]	0.614	0.610	1.405	181.152	.000[b]
Shiraz	Obs-Wind	.610[a]	0.372	0.368	0.842	119.436	.000[b]
	ECMWF-Wind	.224[a]	0.050	0.045	0.944	10.660	.001[b]
	Obs-Rain	.196[a]	0.039	0.034	1.427	8.106	.005[b]
	TRMM-Rain	.261[a]	0.068	0.064	1.186	14.793	.000[b]
	Obs-Tem	.974[a]	0.949	0.949	1.398	5590.350	.000[b]
	Obs-Humidity	.791[a]	0.625	0.624	1.162	497.085	.000[b]

the SSP585 scenario, for both near- and distant-future periods, the maximum rate of increase is projected for autumn (5.94% and 12.49% respectively). This implies greatest expected increase in future wildfires during autumn (Fig. 3).

4.3 Spatiotemporal variability of FWI over the study region

Based on the proposed classification of FWI thresholds, a six-level classification for FWI was introduced (Table 1), and based on these proposed classes, the study area for both reference and future periods was categorized. Notably, the annual average of this index serves as the basis for interpreting our results. As observed in Fig. 4, for the "very low" class using the SSP245 scenario, there is no

		SSP245			SSP585			Min
	Season	1960-2020	2031-2060	2061-2090	1960-2020	2031-2060	2061-2090	
Seasonal average	DJF	4.14	5.91	6.57	4.12	5.71	6.68	
	MAM	15.9	17.49	17.44	15.65	16.81	16.56	
	JJA	48.71	51.98	53.14	48.58	52.38	54.91	
	SON	32.28	33.96	36.01	32.24	34.65	38.27	
Seasonal frequency (%)	DJF	0.06	0.16	0.2	0.07	0.36	0.46	
	MAM	12.68	14.12	12.92	12.43	12.06	11.14	
	JJA	81.39	85.62	86.07	81.21	84.82	85.72	
	SON	41.94	46.06	50.32	41.69	47.63	54.18	Max

Fig. 3 Seasonal average FWI and percentage of seasonal FWI > 38 considering the time series of the reference period and future data

occurrence during the study periods, and only 0.37% of the study area falls into the "low" category during the reference period. However, the area of "moderate" class increases compared to the two previous classes (24.19% during the reference period and 13.04% and 11.37% for the near- [2031–2060] and distant- [2061–2090] futures respectively). The "high" class area shows a higher value for the near- (86.97%) and distant- (83.49%) futures, compared to the reference period (75.45%). Additionally, only a small portion of the area (5.15%) falls within the "very high" class in the distant future, while no areas are projected for the "extreme" class.

Our results for the SSP585 scenario are similar to those for the SSP245 scenario. For SSP585, no areas occur in the "very low" class, and only 0.43% of the area falls within the "low" category during the reference period. Moreover, the "moderate" class covers 25.03% of the area during the reference period, and 13.10% and 9.88% for the near- and distant-futures respectively. The largest area belongs to the "high" class in the SSP585 scenario, with 86.90% and 86.14% for the near- and distant-futures respectively, compared to 74.55% for the reference period. While none of the areas have their annual averages within the "extreme" class, 3.98% of the Zagros region falls within the "very high" class during the distant-future. From a spatial distribution perspective, the outputs of all scenarios demonstrate that the minimum annual average FWI is located in the northwestern Zagros, with the maximum annual average FWI experienced moving towards its southeast (Fig. 5).

Our findings suggest that under the influence of climate change (i.e. warming, drying) in future decades, the area associated with some frequency classes will increase. According to SSP245 scenario results, there is expected to be a 3.47% areal increase associated with a 41–80 day frequency threshold for the near-future, and a 0.60% increase within the 81–120 day class in the distant-future. Projected areal increase associated with the 121–160 day class is 4.75% for the near-future, while that for the 161–200 day class is 3.94% for the near-future and 1.28% for the distant-future, compared to the reference period (Fig. 6).

For all study periods, the lowest FWI frequencies are observed in the northwestern region where frequencies of 11–60 days per annum are recorded (Fig. 7). However, FWI frequencies of 120–160 days per annum are evident for central areas, and up to 160–200 days per annum for southeastern areas (Fig. 7).

For the SSP245 scenario, maximum near-future FWI increases of 20–30 and 30–40 days per annum are projected for the northwestern area. Significant portions of the central and southeastern areas are expected to experience only minor FWI increases ranging from 4 to 10 days per annum. However, projected distant-future changes indicate that the northwestern area will continue to experience the highest rate of FWI increase (30–50 days per annum), but decreases in rate towards southeastern areas. Moreover, model outputs indicate that the lowest rate of increase (4–10 days per annum) is expected in localities within the eastern central to southeastern areas (Fig. 8).

For SSP585 scenario outputs, FWI areal increases are modelled for classes of 41–80 days per annum (near-future; 3.50%), 81–120 days per annum (distant-future; 1.73%), and 121–160 days per annum (near-future; 6.16%) (Fig. 6). For all study periods, the lowest frequency rates of extreme values (FWI > 38) are observed in northwestern regions (Fig. 7). For the reference period, this threshold ranges between 11 and 40 days per annum, while for the near- and distant-futures, it includes thresholds of 40–80 and 80–100 days per annum respectively. However, from a general perspective encompassing results from all-time series, it is evident that in central regions, the threshold of 120–160 days per annum dominates. This expands towards southern and southeastern areas, where the frequency increases to a threshold of 181–200 days per annum (Fig. 7). Spatially, the pattern of this scenario is almost identical to that for SSP245 scenarios. It is notable that for both near- and distant-future periods, the maximum rate of FWI increase occurs in northwestern areas. Apart from the northwestern area, other study areas are projected to experience an increase in FWI of between 4 and 10 days per annum (Fig. 8). However, for the distant future, this rate decreases with expansion towards southern and southeastern areas, apart from increases in concentrated smaller portions of the southeastern area (Fig. 8).

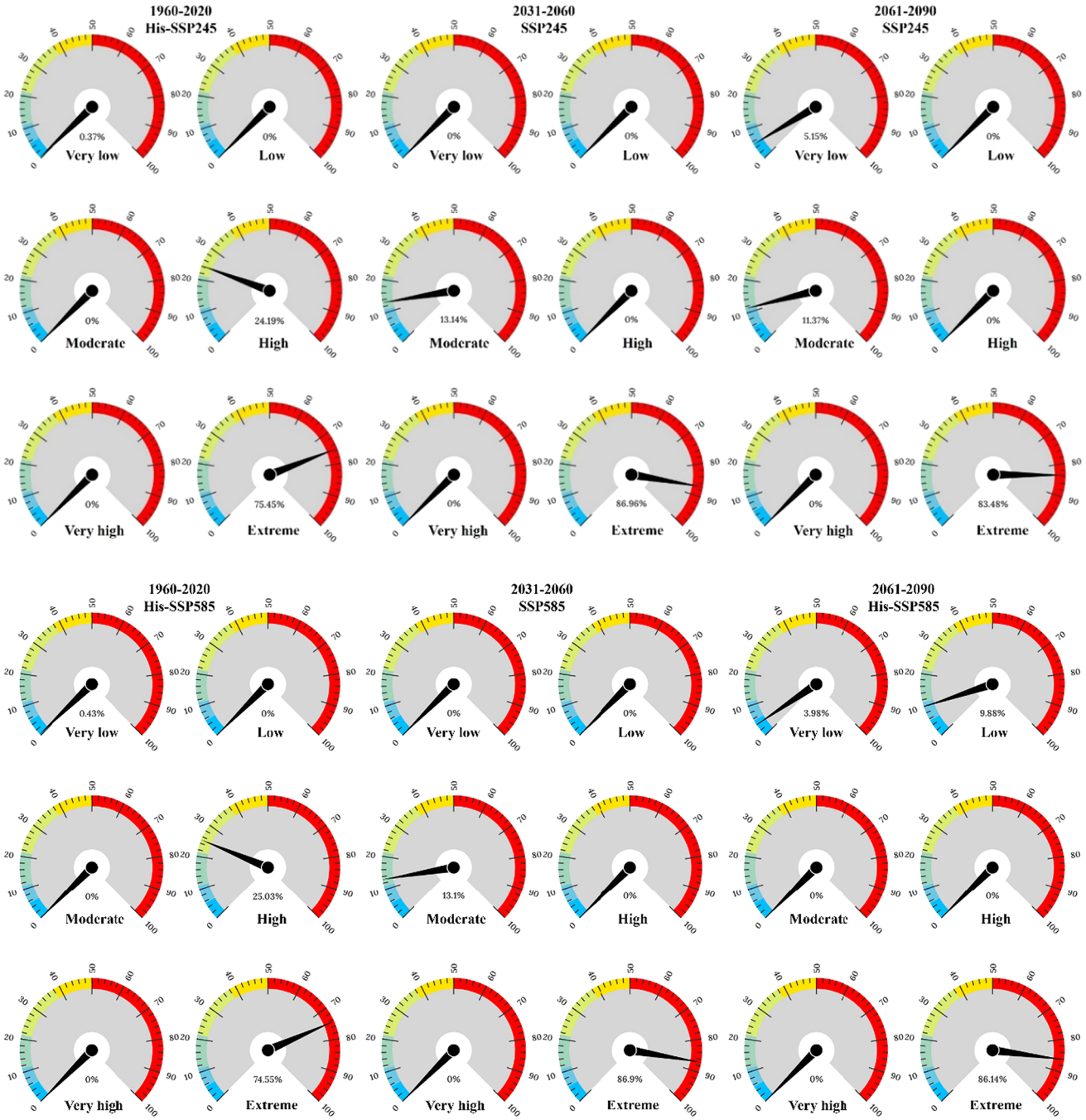


Fig. 4 Comparison of the area corresponding to the annual average of different FWI classes based on the temporal series of the reference period and future data

4.4 Fire warning in forested areas

Figure 9 illustrates the spatial distribution of land use patterns over different periods of time. The reference period data encompass land-use over the period 1992–2020. For our four study periods, the predominant land-use cover is cropland (38.85% of total area). Other dominant land-use types include dense and open forests (31.52%) and bare areas (22.51%) (Fig. 10). During the near- future (2031–2060), croplands continue to dominate, increasing in area by 1.12%, whilst bare areas are projected to increase by 3.7%, but dense and open forests decrease by 4.9%. For the distant-future, croplands continue to expand (reaching 41.2% of total area), as do bare areas (to 28.83% of total area), but dense and open forests decline by 9%, representing only 22.9% of the total area (Fig. 10).

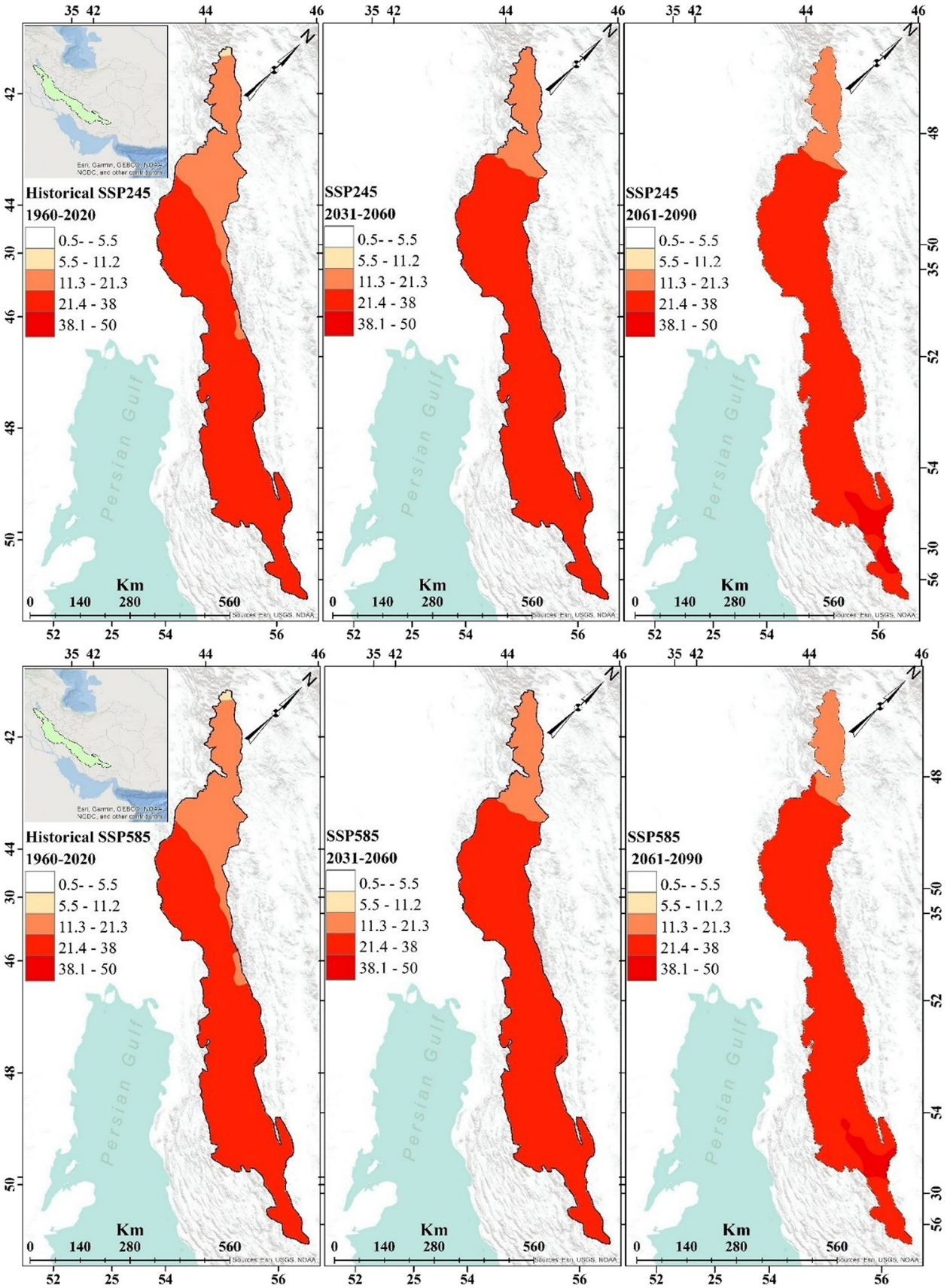


Fig. 5 Spatial distribution of the annual average FWI considering the reference period and future data series

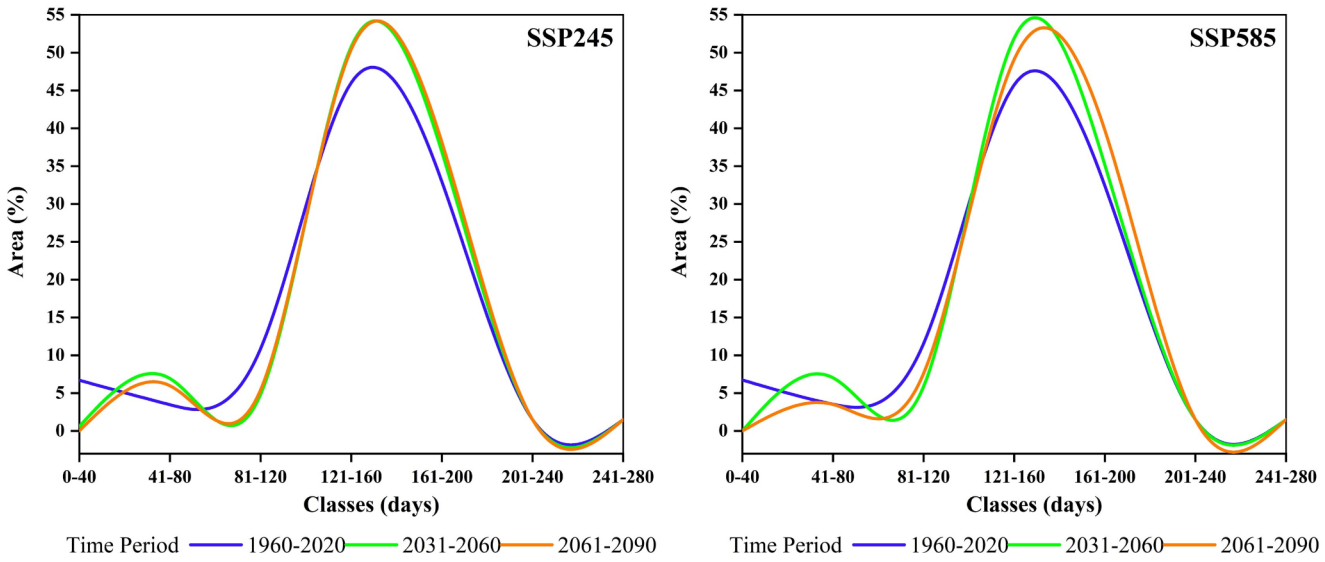


Fig. 6 Comparison of the area corresponding to the average annual frequency of FWI > 38 based on the time series of the reference period and future data in scenarios SSP245 and SSP585

Spatially, croplands dominate northwestern areas, while sparser forest coverage is evident in this region. In the central area, dense and open forests initially prevail, followed by bare areas and croplands. In the southeast, bare areas dominate (Fig. 9).

Our findings indicate that for the reference period (1992–2020), the FWI averages 26.27 and 26.07 for SSP245 and SSP585, respectively. However, for the near future, the average FWI for both scenarios has reached the maximum value compared to other periods, with values of 28.87 for SSP245 and 28.88 for SSP585, showcasing a slight difference between the two scenarios.

For the distant-future, annual FWI values average 27.93 for SSP245 and 28.78 for SSP585 (Fig. 11a). The average number of days per annum experiencing FWI values > 38 is determined. The reference period records the lowest occurrences, with values of 142.52 and 141.59 days per annum for SSP245 and SSP585, respectively. Notably, the maximum frequency of extreme values is anticipated during the near future, with 153.73 days per annum for SSP245 and 151.94 days per annum for SSP585. Although the frequency rates decrease in the distant-future, compared to the near-future, SSP245 still exhibits higher frequencies (147.56 days per annum) compared to SSP585 (149.21 days per annum) (Fig. 11b).

4.5 FWI changes and elevation

It is evident that the highest annual average FWI is associated with elevation categories of less than 1000 m asl, predominantly in the western parts of the study region (Fig. 12). Although the annual average FWI for elevation categories below 1000 m asl exceeds that of other elevations, there is an increasing trend observed for elevations > 1000 m asl.

The average annual rate of FWI change for both near- and distant-futures, applying SSP245 and SSP585 scenarios, indicates that the rate of increase for all elevation categories is higher in the distant-future, compared to the near-future. The most pronounced increase in FWI (using the SSP245 scenario) is projected for elevations between 1000 and 2000 m asl (3.11 for both near and distant futures). In contrast, when applying the SSP585 scenario, maximum changes (4.30) are projected for elevations below 1000 m asl (Fig. 12). Due to ongoing projected climate warming in forthcoming decades, the fire occurrence will increase at all elevations but will be most pronounced for the distant future (i.e., 2061–2090) at elevations of 1000–2000 m asl (Fig. 13).

4.6 FWI trends

The annual frequency of days exceeding the specified FWI > 38 threshold for each year was calculated, and the median of the data determined for each decade. FWI trends are established for a time series comprising 18 records over the period 1960–2090. Our results demonstrate no decreasing trends in FWI. The most significant and meaningful increases in FWI are observed for northwestern and central regions (Fig. 14). According to the SSP245 scenario, 28.83% of the study area has not experienced any significant trend, but when applying the SSP585 scenario, only 1.80% of the area has not experienced any significant trend. SSP245 shows that 15.32% and 50.45% of the area experiences an

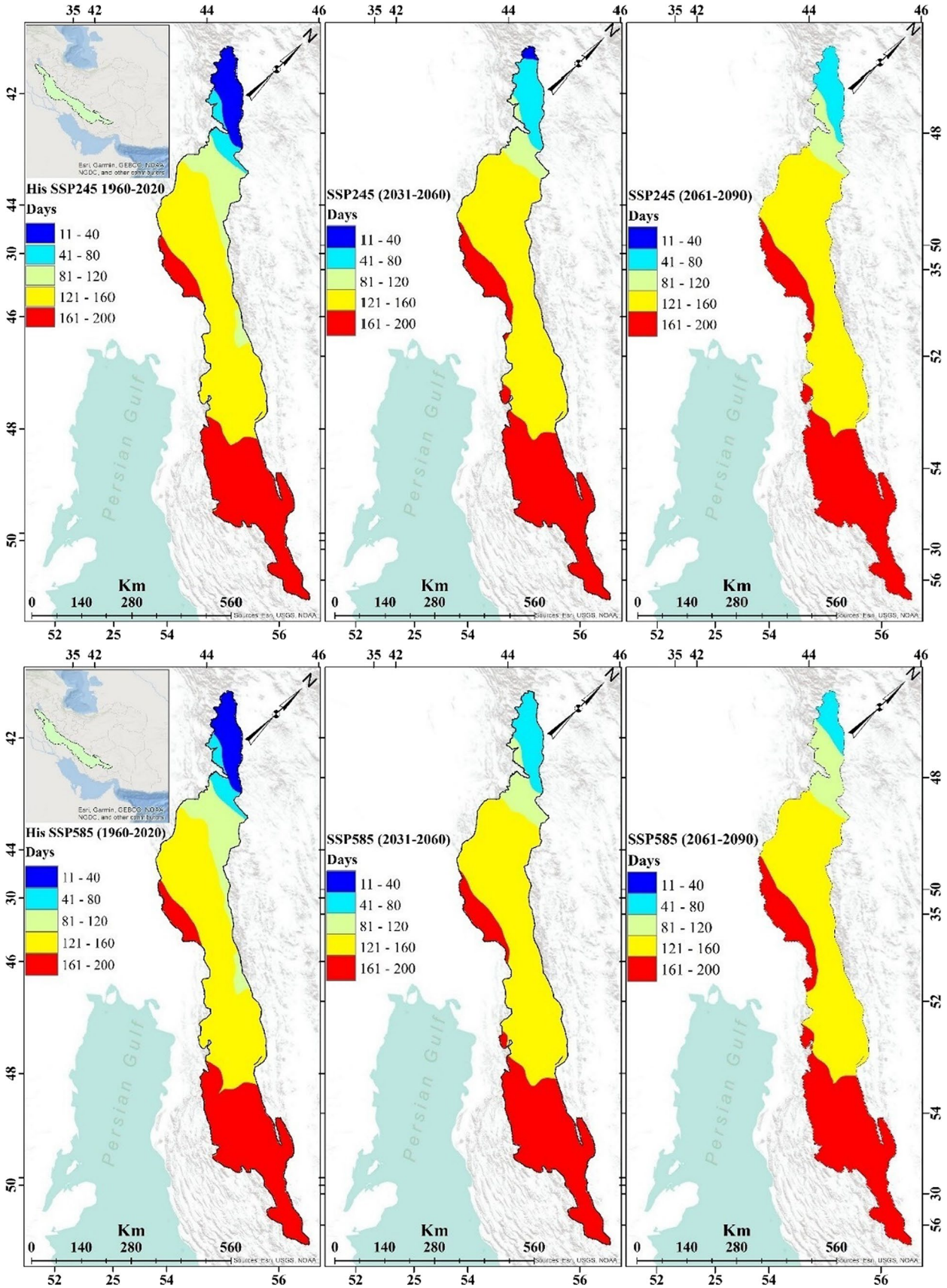


Fig. 7 Comparison of the spatiotemporal distribution of the average number of days per year with FWI > 38 for the reference and future periods

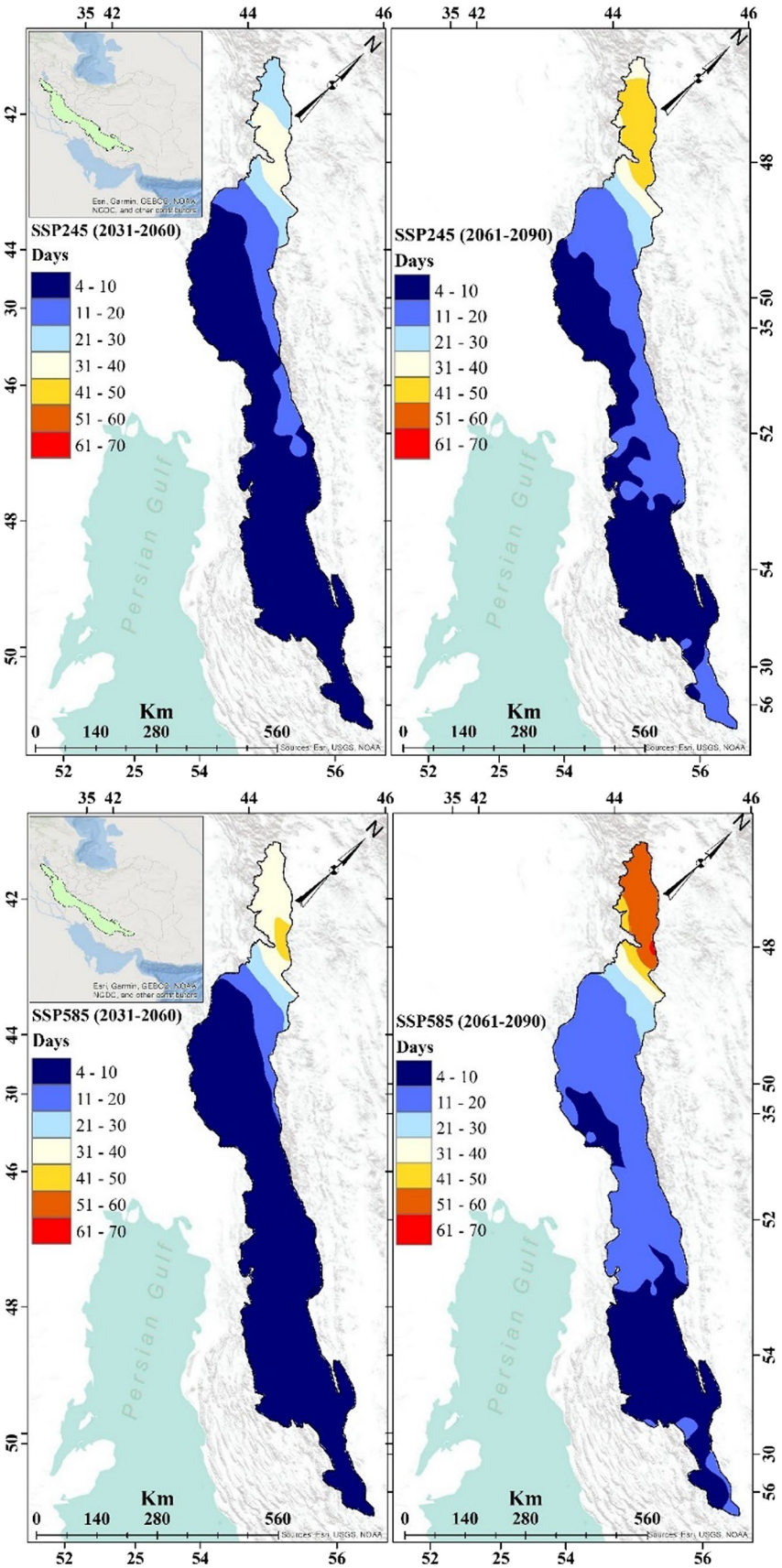


Fig. 8 Daily frequency (average number of days per annum) of FWI > 38 values for future decades, relative to the reference period

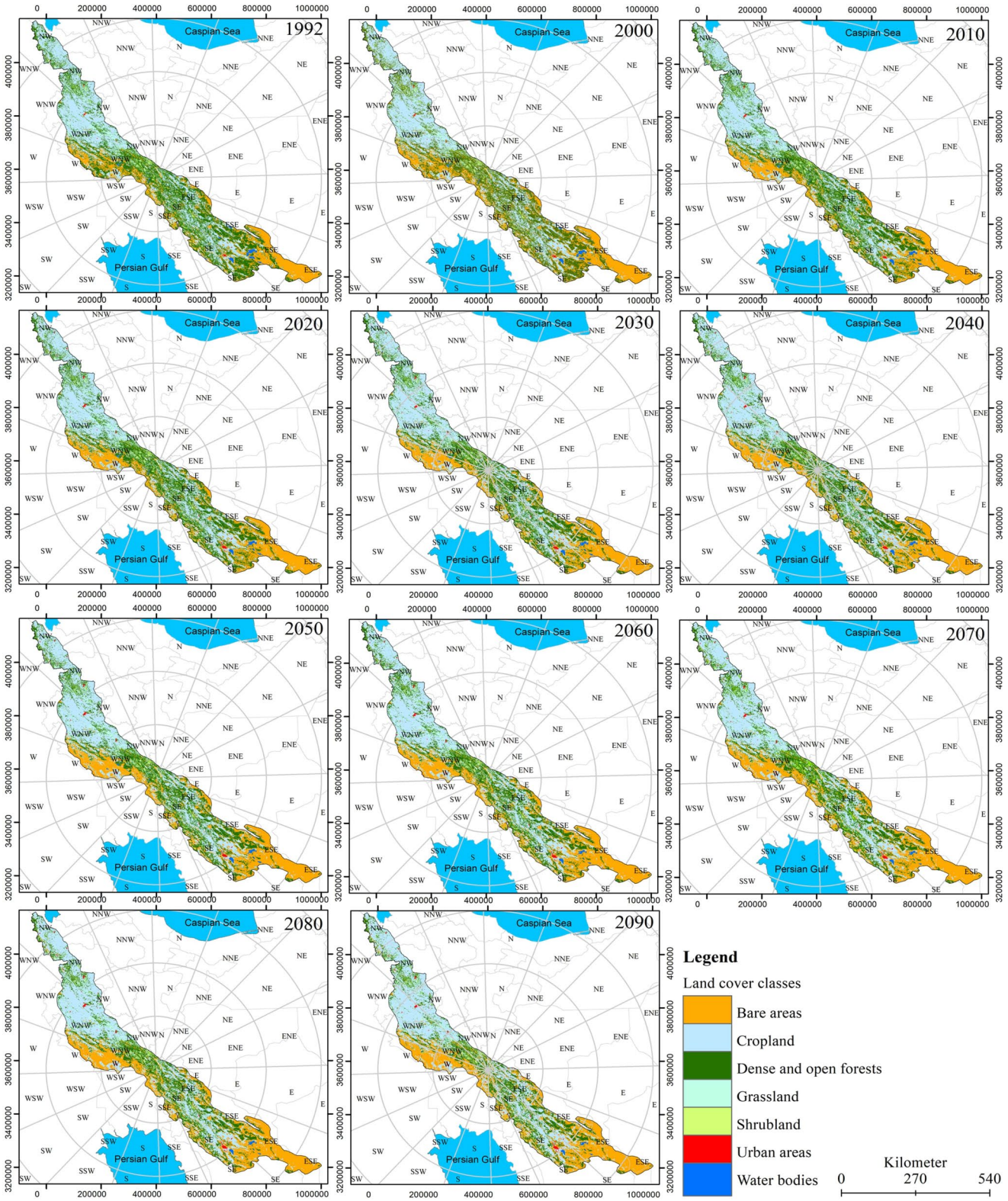
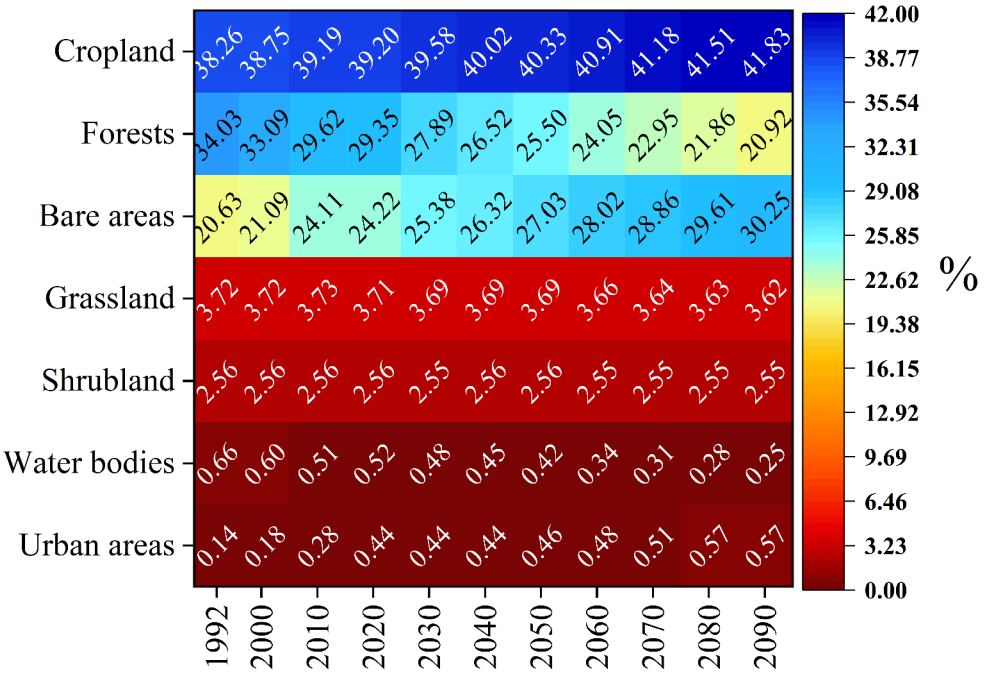


Fig. 9 Spatiotemporal changes in land use across the Zagros region during the study period: 1992–2090



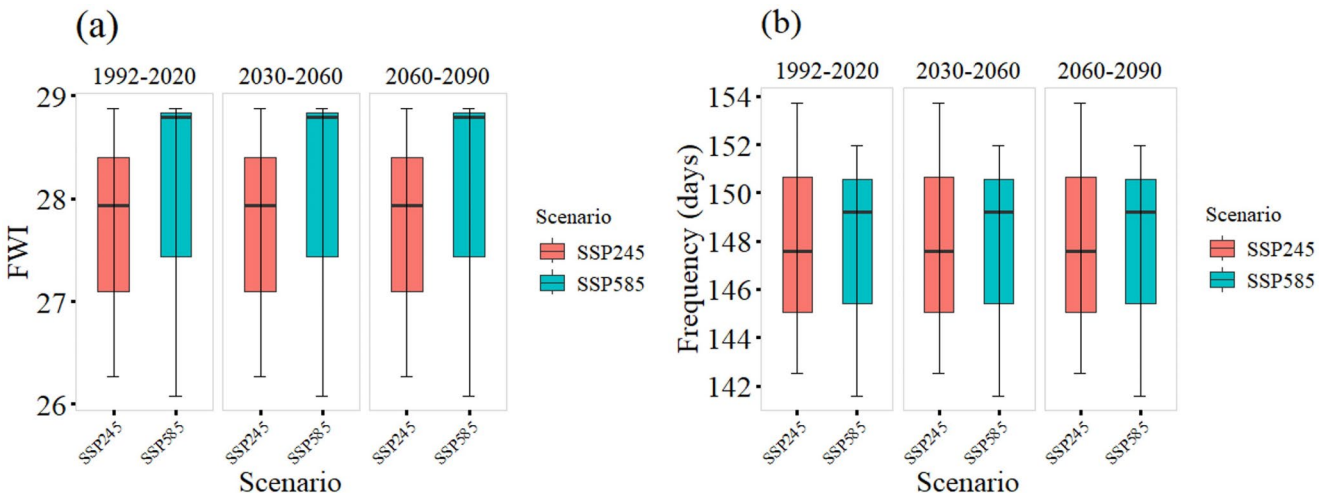


Fig. 10 Percentage land use cover for different periods of time

Fig. 11 **a** Comparison of annual average FWI and **b** average frequency of days per year with FWI > 38 values based on time series of dense and open forests land use areas

increase with confidence levels of 95% and 99% respectively, while SSP585 records 18.02% and 72.97%, respectively. Overall, 65.8% of SSP245 and approximately 91% of SSP585 exhibit a significant increasing trend (above the 95% level), indicating a higher intensity and extent in the SSP585 scenario (Table 6).

4.7 Temporal and spatial changes of emerging hot spots of FWI

Using the Emerging Hot Spot Analysis (EHSA) tool, spatiotemporal changes in FWI are now investigated. For this, FWI includes values greater than the threshold value of 38. Although 17 classes are introduced for EHSA, based on our time series data, only 9 classes are relevant to our region (Table 2). For these 9 classes, occurrence patterns occur for only one of the scenarios for 5 classes, and for the remaining 4 classes, occurrence patterns can be observed for both scenarios. Among these 5 classes, Historical Cold Spot, New Hot Spot, and Oscillating Hot Spot are experienced only for SSP585, while the patterns of Persistent Hot Spot and Sporadic Cold Spot exist only for SSP245 (Fig. 15; Table 7).

The spatial pattern of EHSA changes indicates that in both scenarios, a Diminishing Cold Spot pattern concentrated over the northwestern area, accounts for

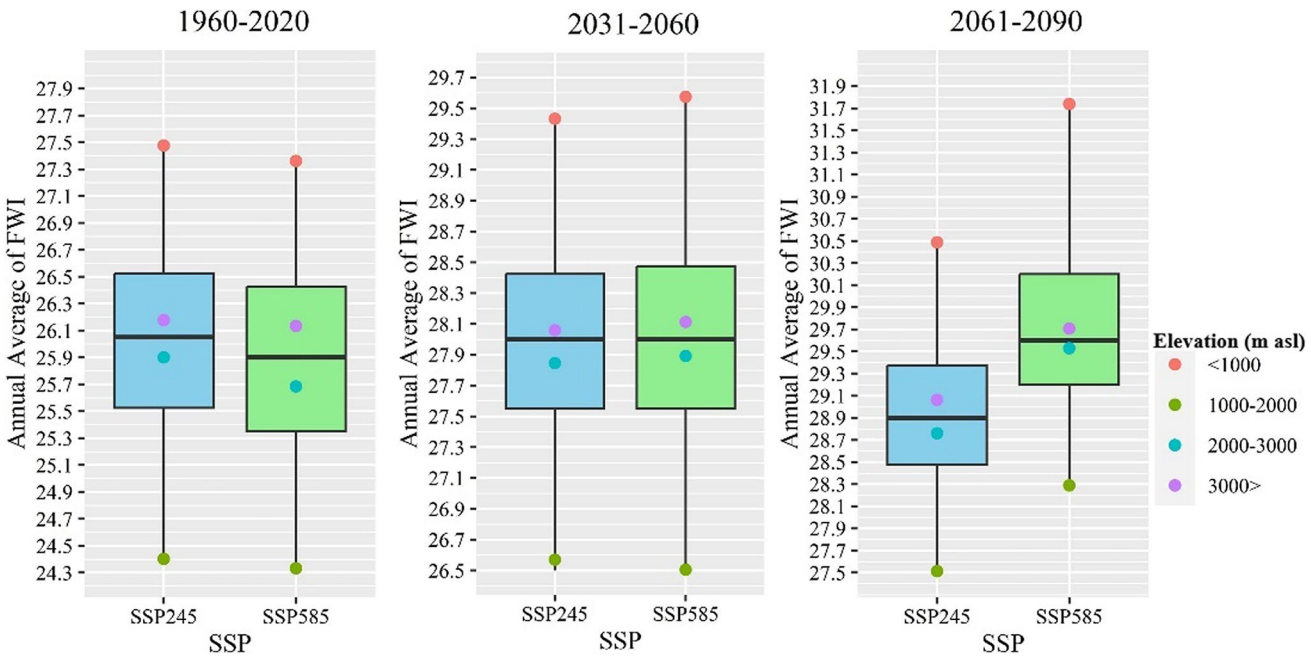


Fig. 12 The mean annual FWI for elevation classes from < 1000 m asl to > 3000 m asl considering the reference period and future data series

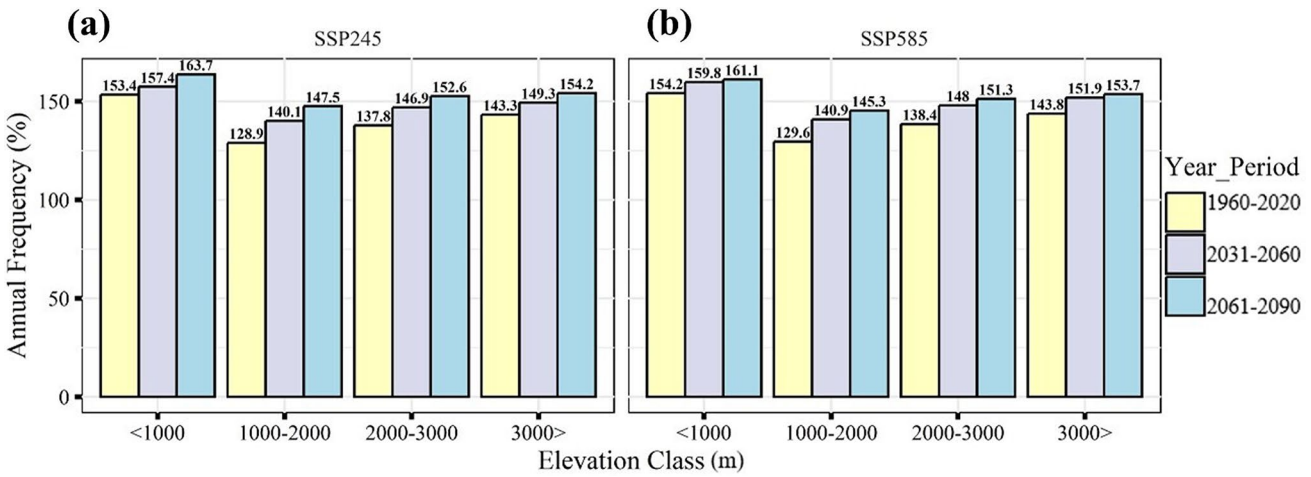


Fig. 13 The percentage annual frequency of FWI > 38 based on different elevation classes for **a** SSP245 and **b** SSP585

9% (SSP245 scenario) and 14.4% (SSP585 scenario). Towards lower latitudes, the Sporadic Cold Spot pattern is observed over 2.7% of the area (SSP245 scenario), while for the SSP585 scenario, this is 1.8% of the area. For most central areas, the outcome is 'No Pattern Detected', covering 45.9% of the area for SSP245 and 32.4% of the area for SSP585. The Consecutive Hot Spot pattern in SSP245 appears as two zones, one in the central area and the other in the southeast, covering 9% of the total area. However, for SSP585, this pattern of occurrence is scattered into three separate zones from the central to southern areas, covering a total of 14.4% of the area. In SSP245, two different classes are concentrated over the southern and southeastern regions, one being Persistent Hot Spot (21.6% of total area) and the other Intensifying Hot Spot (5.4% of total area). The SSP585 outputs indicate that the most important pattern in the southern and southeastern regions belongs to the Intensifying Hot Spot class, covering 27% of the Zagros region (Fig. 15; Table 7).

5 Discussion

Our results demonstrate that weather-related fire danger will expand spatially across the Zagros Mountains in both the near- and distant-futures according to both SSP scenarios (245 or 585).

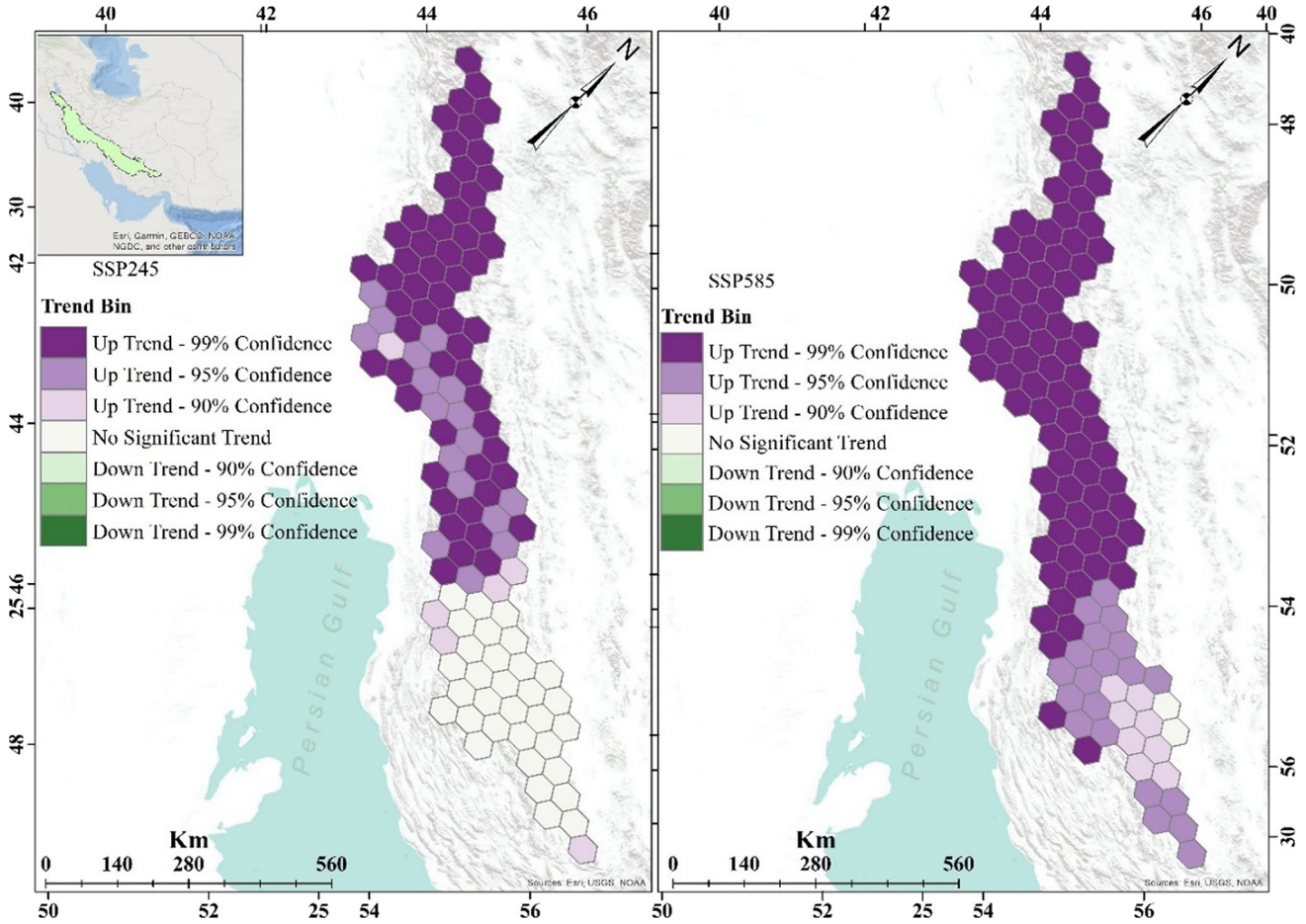


Fig. 14 Changes in FWI (> 38) over the Zagros Mountains using the Mann–Kendall method

Table 6 Significant levels of change in the FWI (> 38), using the Mann–Kendall test

The significance level	Trend_BIN	SSP245-Area (%)	SSP585-Area (%)
Down Trend – 99% Confidence	-3	0	0
Down Trend – 95% Confidence	-2	0	0
Down Trend – 90% Confidence	-1	0	0
No Significant Trend	0	28.83	1.80
Up Trend – 90% Confidence	1	5.4	7.2
Up Trend – 95% Confidence	2	15.3	18.0
Up Trend – 99% Confidence	3	50.5	73.0

Findings indicate that the long-term annual average FWI for some areas in the distant future (2061–2090) is likely to fall within the "very high" danger class. Moreover, the frequency of extreme FWI > 38 occurrences is projected to increase across the entire study region. Although the lowest annual average FWI and the lowest frequency of extreme FWI values during the reference period were observed in northwestern areas of our Zagros study region, the largest increase in FWI > 38 is projected for this region in the context of global warming. Our Mann-Kendall results also indicate a significant and increasing trend in FWI for the northwestern region, which significantly coincides with the occurrence of Diminishing Cold Spot patterns, thus adding confidence in our FWI projections. Numerous studies worldwide have reported a similar future projection and increasing trends in wildfires, including research conducted in Iberia (Bento et al. 2023), the Attica region in Greece (Politi et al. 2023), the United States of America (Vose et al., 2012; Kookhaie et al., 2014; Varela et al., 2019), the French Mediterranean region in Provence-Alpes-Côte d'Azur, Spain (Moreno et al. 2023), Korea (Chang et al. 2024), and Africa (Justino et al. 2013).

Notable similarities and differences exist between our findings and those of previous research examining the relationships between climatic variables and their impacts on fire risk. For instance, in alignment with our findings from the Zagros region, Krikken et al. (2021) attribute the rise in forest fires in Sweden to climate change, indicating that global warming substantially contributes to fire danger. Similarly, findings from western- (Iberia) and eastern- Europe have advocated that

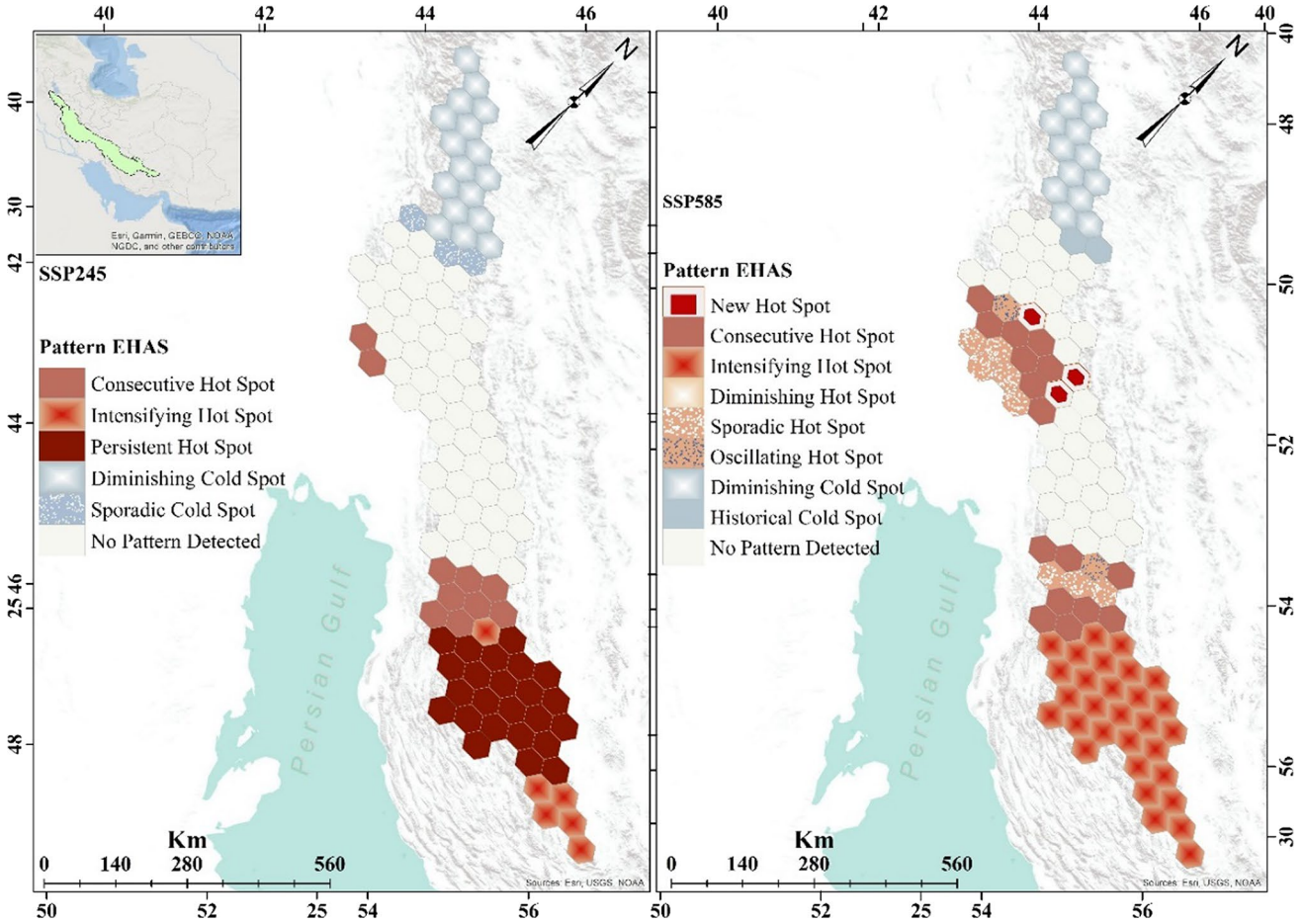


Fig. 15 Spatiotemporal anomalies of FWI (> 38) over the Zagros Mountains using EHSA analysis

Table 7 Area related to FWI (> 38) anomalies according to each of the EHSA patterns

Row	Pattern	SSP245	SSP585
1	Consecutive Hot Spot	9.01	14.41
2	Diminishing Cold Spot	15.32	12.61
3	Historical Cold Spot	0.00	1.80
4	Intensifying Hot Spot	5.41	27.03
5	New Hot Spot	0.00	2.70
6	No Pattern Detected	45.95	32.43
7	Oscillating Hot Spot	0.00	1.80
8	Persistent Hot Spot	21.62	0.00
9	Sporadic Cold Spot	2.70	0.00

recent temperature increases, altered precipitation patterns and more prolonged droughts have contributed to an enhanced frequency of 'fire weather' and heightened fire danger (Semenova and Sumak 2022; Bento et al. 2023). In contrast, Jones et al. (2022) present a broader analysis of global and regional drivers of fire under climate change, identifying various factors, including land use and vegetation changes. Their work underscores the importance of localized studies, like ours, in providing valuable insights into specific regional impacts. Additionally, regional assessments in France have linking fire danger projections to other changing climate variables, such as wind speed and relative humidity (Varela et al., 2019; Fargeon et al. 2020). While acknowledging the role of global warming, they emphasize some uncertainties when using climate models for establishing future fire occurrence (risk). Notwithstanding such caution, these studies collectively reinforce the understanding that contemporary climate change, accelerated by global warming, significantly heighten fire occurrence and associated hazards. The alignment of our findings with those of previous work from other regions, further reinforces that 'fire weather' patterns are not only increasing in frequency, but also expanding spatially.

Climate change impact over Iran is highly variable given diversity in topography and atmospheric systems over the region (Hamidi et al. 2024; Alijani 2002; Daneshvar et al., 2019). For instance, it has been demonstrated that geographical factors (longitude/latitude, elevation, distance from oceans) have varied climatic influence and hence responses to climate warming in future decades (Ghanghermeh et al. 2022). The Zagros

Mountains extend northwest to southeast, causing significant differences in longitude (distance from the Persian Gulf) and latitude. It has been established that temperatures have increased in recent decades over the Alborz Mountains, but that these have varied elevationally and latitudinally due to irregularity of lapse rates across the region (Roshan et al., 2024a; Roshan et al. 2024b). Similar work has also projected that longitude (continentality) will have an increasing climatic influence on solar radiation patterns in the distant future (2061–2080) (Roshan et al., 2023). These factors in combination, account for spatially variable susceptibilities to future climate change over these mountains (Masoodian and Keikhosravi Kiany 2020; Arsalani et al. 2022; Mohimi and Esmaeily 2023; Sadrianzadeh et al., 2023). The cumulative effects of these variable projected climatic changes over time, will then most likely also influence future wildfire patterns and danger in the region. In this study, for the first time, we used emerging hotspot analysis to reveal spatio-temporal changes of different patterns of cold and hot spots for forest fire danger. To this end, in our comparison between the two scenarios of SSP245 and SSP585, we found that the patterns related to EHA for SSP585 had more diversity compared to SSP245. Examining the climatic data for each SSP scenario could offer a deeper understanding of the differences in input data originating from the SSPs. However, such analysis falls outside the scope of the current research.

Land use change is among the most influential and important factors affecting the diversity of EHA patterns. One of the most impacted land use types by wildfires is forested areas. We find that the percentage of land allocated to this land use type will decrease in future decades. This conclusion is made under the assumption that the impact of wildfires on the rate of decline in this land use type will increase, and thus one can expect less future forested areas in this study region. This poses a significant danger to the ecosystem of the Zagros region, leading to considerable adverse environmental consequences such as loss of biodiversity, potential increased soil erosion and slope instability.

Notwithstanding the value of our findings, we acknowledge that there are study limitations that need to be recognized. Firstly, the downscaled climate models may overlook localized microclimates, particularly in the complex terrains of the Zagros Mountains. The limited validation, based on only eight meteorological stations and two satellite datasets, introduces uncertainties that could affect the reliability of the model outputs. Moreover, while focusing on fire weather indices is essential, it fails to consider other crucial elements like forest management and socio-economic factors that influence fire dynamics. The exclusive use of two Shared Socioeconomic Pathway scenarios restricts the exploration of diverse future climate scenarios, limiting the comprehensiveness of the findings. Additionally, relying solely on the Fire Weather Index may oversimplify the intricate relationships between climate, vegetation, and fire behavior. Finally, omitting indices related to drought and heatwaves restricts a holistic understanding of the future fire danger landscape. Each of these limitations highlights the need for more robust models and broader considerations to enhance the accuracy and applicability of the study's conclusions.

6 Conclusion

This study has investigated the impact of climate change on fire danger in the Zagros Mountains for near- and distant-futures. This has been achieved through utilizing climate model simulations under two Shared Socioeconomic Pathway (SSP) scenarios. These scenarios are based on assumptions regarding socioeconomic and land-use changes. The findings presented here thus offer insights into *potential* changes in fire danger and provide a foundation for designing management strategies aimed at fire prevention and mitigation in the area.

The future potential for increased wildfire risk in the Zagros region can be attributed to various atmospheric factors. Climate warming and longer drought periods or dry spells accelerate the desiccation of vegetation and enhance the flammability of combustible materials. Additionally, global warming also contributes to greater atmospheric instability (e.g. Rädler et al. 2019), resulting in more frequent thunderstorms that can ignite wildfires through higher lightning flash density.These interconnected atmospheric factors underscore the significance of our findings, emphasizing the need for proactive measures to mitigate future wildfire risks.

Priority should be given to developing and implementing fire alarm systems tailored to the geographic and climatic conditions of the study region. Future research will focus on utilizing Regional Climate Models (RCMs), driven by outputs from various Global Climate Models (GCMs), to assess bias patterns and signals of climate change more efficiently. Future work should additionally incorporate drought and heat wave indices for establishing fire danger.

Author contributions Conceptualization, G.R.R.; methodology, G.R.R., A.A.G., M.A.E., R.S.; software, A.A.G., M.A.E., R.S.; validation, A.A.G.; formal analysis, G.R.R., investigation, G.R.R., and A.A.G.; data curation, A.A.G., and R.S.; writing—original draft preparation, G. R. R.; writing—review and editing, G.R.R., and S. W.G.; visualization, S.W. G.; supervision, G.R.R.; project administration, G.R.R. and A.A.G.; All authors have read and agreed to the published version of the manuscript.

Data availability No datasets were generated or analysed during the current study.

Declarations

Conflict of interest The authors declare no competing interests.

References

Abney RB, Sanderman J, Johnson D, Fogel ML, Berhe AA (2017) Post-wildfire erosion in mountainous terrain leads to rapid and major redistribution of soil organic carbon. Front Earth Sci 5. https://doi.org/10.3389/feart.2017.00099

Ahmadi R, Asemani M, Hamidi N, Rezaei SS, Ahmadi A, Amirahmadi F, Aghaei S, Bayat F (2024) Analyzing the relationship between place attachment and residential satisfaction through the mediation of social capital- the case of affordable housing. J Housing Built Environ. https://doi.org/10.1007/s10901-024-10146-1

Alijani B (2002) Variations of 500? hPa flow patterns over Iranand surrounding areas and their relationship with the climate of Iran. Theoret Appl Climatol 72(1–2):41–54. https://doi.org/10.1007/s007040200011

Allen CD, Macalady AK, Chenchouni H, Bachelet D, McDowell N, Vennetier M, Kitzberger T, Rigling A, Breshears DD, Hogg E, Gonzalez P, Fensham R, Zhang Z, Castro J, Demidova N, Lim J, Allard G, Running SW, Semerci A, Cobb N (2009) A global overview of drought and heat-induced tree mortality reveals emerging climate change risks for forests. For Ecol Manag 259(4):660–684. https://doi.org/10.1016/j.foreco.2009.09.001

Arsalani M, Grießinger J, Bräuning A (2022) Tree-ring-based seasonal temperature reconstructions and ecological implications of recent warming on oak forest health in the Zagros Mountains, Iran. Int J Biometeorol 66(12):2553–2565. https://doi.org/10.1007/s00484-022-02380-5

Ascoli D, Plana E, Oggioni SD, Tomao A, Colonico M, Corona P, Giannino F, Moreno M, Xanthopoulos G, Kaoukis K, Athanasiou M, Colaço MC, Rego F, Sequeira AC, Acácio V, Serra M, Barbati A (2023) Fire-smart solutions for sustainable wildfire risk prevention: Bottom-up initiatives meet top-down policies under EU green deal. Int J Disaster Risk Reduct 92:103715. https://doi.org/10.1016/j.ijdrr.2023.103715

Barnes ML, Zhang Q, Robeson SM, Young L, Burakowski EA, Oishi AC, Stoy PC, Katul G, Novick KA (2024) A century of reforestation reduced anthropogenic warming in the eastern United States. Earth S Future 12(2). https://doi.org/10.1029/2023ef003663

Bedia J, Herrera S, Gutiérrez JM, Benali A, Brands S, Mota B, Moreno JM (2015) Global patterns in the sensitivity of burned area to fire-weather: Implications for climate change. Agric For Meteorol 214–215. https://doi.org/10.1016/j.agrformet.2015.09.002

Bento VA, Lima DC, Santos LC, Lima MM, Russo A, Nunes SA, DaCamara CC, Trigo RM, Soares PM (2023) The future of extreme meteorological fire danger under climate change scenarios for Iberia. Weather Clim Extremes 42:100623. https://doi.org/10.1016/j.wace.2023.100623

Bett PE, Williams KE, Burton C, Scaife AA, Wiltshire AJ, Gilham R (2020) Skillful seasonal prediction of key carbon cycle components: NPP and fire risk. Environ Res Commun 2(5):055002. https://doi.org/10.1088/2515-7620/ab8b29

Bulkeley H, Newell P (2011) Governing climate change. Choice Reviews Online 48(07):48–4109. https://doi.org/10.5860/choice.48-4109

Campos I, Abrantes N, Keizer JJ, Vale C, Pereira P (2016) Major and trace elements in soils and ashes of eucalypt and pine forest plantations in Portugal following a wildfire. Sci Total Environ 572:1363–1376. https://doi.org/10.1016/j.scitotenv.2016.01.190

Carpio-Pinedo J, Romanillos G, Aparicio D, Martín-Caro MSH, García-Palomares JC, Gutiérrez J (2022) Towards a new urban geography of expenditure: using bank card transactions data to analyze multi-sector spatiotemporal distributions. Cities 131:103894. https://doi.org/10.1016/j.cities.2022.103894

Carta F, Zidda C, Putzu M, Loru D, Anedda M, Giusto D (2023) Advancements in forest fire prevention: a comprehensive survey. Sensors 23(14):6635. https://doi.org/10.3390/s23146635

Carvalho A, Flannigan MD, Logan KA, Gowman LM, Miranda AI, Borrego C (2009) The impact of spatial resolution on area burned and fire occurrence projections in Portugal under climate change. Clim Change 98(1–2):177–197. https://doi.org/10.1007/s10584-009-9667-2

Chang S, Wang Z, Mao D, Guan K, Jia M, Chen C (2020) Mapping the essential urban land use in Changchun by applying random forest and Multi-Source geospatial data. Remote Sens 12(15):2488. https://doi.org/10.3390/rs12152488

Chang DY, Jeong S, Park C, Park H, Shin J, Bae Y, Park H, Park CR (2024) Unprecedented wildfires in Korea: Historical evidence of increasing wildfire activity due to climate change. Agric For Meteorol 348:109920. https://doi.org/10.1016/j.agrformet.2024.109920

Chungu D, Ng'andwe P, Mubanga H, Chileshe F (2019) Fire alters the availability of soil nutrients and accelerates growth of Eucalyptus grandis in Zambia. J Forestry Res 31(5):1637–1645. https://doi.org/10.1007/s11676-019-00977-y

Daneshvar MRM, Ebrahimi M, Nejadsoleymani H (2019) An overview of climate change in Iran: facts and statistics. Environ Syst Res 8(1). https://doi.org/10.1186/s40068-019-0135-3

de Groot WJ (1987) Interpreting the Canadian forest fire weather index (FWI) system. In: Hirsch KG (ed) 'Proceedings: fourth central regional fire weather committee scientific and technical seminar', 2 April 1987, Winnipeg, Manitoba. Canadian Forestry Service, Northern Forestry Centre, Edmonton, AB, Canada, pp 3–14

de Rigo D (2016) Structure of the Canadian Forest fire weather index system: the model and its components. https://doi.org/10.5281/ZENODO.6558577

Di Giuseppe F, Rémy S, Pappenberger F, Wetterhall F (2018) Using the Fire Weather Index (FWI) to improve the estimation of fire emissions from fire radiative power (FRP) observations. Atmos Chem Phys 18(8):5359–5370. https://doi.org/10.5194/acp-18-5359-2018

Di Napoli M, Marsiglia P, Di Martire D, Ramondini M, Ullo SL, Calcaterra D (2020) Landslide Susceptibility Assessment of Wildfire Burnt Areas through Earth-Observation Techniques and a Machine Learning-Based Approach. Remote Sens 12(15):2505. https://doi.org/10.3390/rs12152505

Dimitrakopoulos AP, Bemmerzouk AM, Mitsopoulos ID (2010) Evaluation of the Canadian fire weather index system in an eastern Mediterranean environment. Meteorol Appl 18(1):83–93. https://doi.org/10.1002/met.214

Eastman JR (2003) IDRISI Kilimanjaro Tutorial. ManualVersion 14.0. Worcester, Massachusetts: Clark Labs of ClarkUniversity, 61–123.https://web.pdx.edu/~bjpd/courses/g424/KilimanjaroTutorial.pdf

Eskandari S, Chuvieco E (2015) Fire danger assessment in Iran based on geospatial information. Int J Appl Earth Obs Geoinf 42:57–64. https://doi.org/10.1016/j.jag.2015.05.006

ESRI. How Emerging Hot Spot Analysis Works (2023) Available online: https://pro.arcgis.com/en/pro-app/latest/tool-reference/s

pace-time-pattern-mining/learnmoreemerging.htm (accessed on 16 May 2023)
Fan F, Wang Y, Wang Z (2007) Temporal and spatial change detecting (1998–2003) and predicting of land use and land cover in Core corridor of Pearl River Delta (China) by using TM and ETM + images. Environ Monit Assess 137(1–3). https://doi.org/10.1007/s10661-007-9734-y
Fargeon H, Pimont F, Martin-StPaul N, De Caceres M, Ruffault J, Barbero R, Dupuy J (2020) Projections of fire danger under climate change over France: where do the greatest uncertainties lie? Clim Change 160(3):479–493. https://doi.org/10.1007/s10584-019-02629-w
Fujioka FM, Gill AM, Viegas DX, Wotton BM (2008) Chapter 21 Fire Danger and Fire Behavior Modeling Systems in Australia, Europe, and North America. In Developments in environmental science (pp. 471–497). https://doi.org/10.1016/s1474-8177(08)00021-1
Gajendiran K, Kandasamy S, Narayanan M (2023) Influences of wildfire on the forest ecosystem and climate change: a comprehensive study. Environ Res 240:117537. https://doi.org/10.1016/j.envres.2023.117537
Ghaedi Z, Badri S, Saberi-Pirooz R, Vaissi S, Javidkar M, Ahmadzadeh F (2020) The Zagros Mountains acting as a natural barrier to gene flow in the Middle East: more evidence from the evolutionary history of spiny-tailed lizards (Uromasticinae: Saara). Zool J Linn Soc 192(4):1123–1136. https://doi.org/10.1093/zoolinnean/zlaa113
Ghanghermeh A, Roshan G, Halabian A (2022) Projecting spatiotemporal variations of sunshine duration with regards to climate change in Iran as a step towards clean energy. Sustain Energy Technol Assess 53:102630. https://doi.org/10.1016/j.seta.2022.102630
Ghanghermeh A, Roshan G, Asadi K, Attia S (2024) Spatiotemporal analysis of urban heat islands and vegetation cover using emerging hotspot analysis in a humid subtropical climate. Atmosphere 15(2):161. https://doi.org/10.3390/atmos15020161
Ghorbanzadeh O, Blaschke T, Gholamnia K, Aryal J (2019) Forest fire susceptibility and risk mapping using social/infrastructural vulnerability and environmental variables. Fire 2(3):50. https://doi.org/10.3390/fire2030050
Giannakopoulos C, Sager PL, Bindi M, Moriondo M, Kostopoulou E, Goodess C (2009) Climatic changes and associated impacts in the mediterranean resulting from a 2°C global warming. Glob Planet Change 68(3):209–224. https://doi.org/10.1016/j.gloplacha.2009.06.001
Giddens A (2015) The politics of climate change. Policy Politics 43(2):155–162. https://doi.org/10.1332/030557315x14290856538163
Grant E, Runkle JD (2021) Long-term health effects of wildfire exposure: a scoping review. J Clim Change Health 6:100110. https://doi.org/10.1016/j.joclim.2021.100110
Grillakis M, Voulgarakis A, Rovithakis A, Seiradakis KD, Koutroulis A, Field RD, Kasoar M, Papadopoulos A, Lazaridis M (2022) Climate drivers of global wildfire burned area. Environ Res Lett 17(4):045021. https://doi.org/10.1088/1748-9326/ac5fa1
Hamidi N, Kivi SB, Ahmadi R, Asemani M, Ahmadi A, Aghaei S, Ghahremani S, Bayat F (2024) The mediating role of sense of place in relationship between localized social ties and residential satisfaction. J Housing Built Environ. https://doi.org/10.1007/s10901-024-10154-1
Hart TC (2021) Investigating Crime Pattern Stability at Micro-Temporal Intervals: Implications for crime analysis and Hotspot Policing Strategies. Criminal Justice Rev 46(2):173–189. https://doi.org/10.1177/0734016821996785
Jahdi R, Salis M, Alcasena FJ, Arabi M, Arca B, Duce P (2020) Evaluating landscape-scale wildfire exposure in northwestern Iran. Nat Hazards 101(3):911–932. https://doi.org/10.1007/s11069-020-03901-4
Jahdi R, Bacciu V, Salis M, Del Giudice L, Cerdà A (2023) Surface wildfire regime and simulation-based wildfire exposure in the Golestan National Park, NE Iran. Fire 6(6):244. https://doi.org/10.3390/fire6060244
Jansson JK, Hofmockel KS (2019) Soil microbiomes and climate change. Nat Rev Microbiol 18(1):35–46. https://doi.org/10.1038/s41579-019-0265-7
Jones MW, Abatzoglou JT, Veraverbeke S, Andela N, Lasslop G, Forkel M, Smith AJP, Burton C, Betts RA, Van Der Werf GR, Sitch S, Canadell JG, Santín C, Kolden C, Doerr SH, Quéré CL (2022) Global and regional trends and drivers of fire under climate change. Rev Geophys 60(3). https://doi.org/10.1029/2020rg000726
Júnior JS, Paulo JR, Mendes J, Alves D, Ribeiro LM, Viegas C (2022) Automatic forest fire danger rating calibration: exploring clustering techniques for regionally customizable fire danger classification. Expert Syst Appl 193:116380. https://doi.org/10.1016/j.eswa.2021.116380
Justino F, Stordal F, Clement A, Coppola E, Setzer A, Brumatti D (2013) Modelling weather and climate related fire risk in Africa. Am J Clim Change 02(04):209–224. https://doi.org/10.4236/ajcc.2013.24022
Khosravi H, Abrishami M, Mehrian MR, Chamberlain B (2024) The positive impact of transit-oriented-development characteristics on metro station usage: a case study of Tehran's metro stations and TOD index calculation. Cities 148:104840. https://doi.org/10.1016/j.cities.2024.104840
Kookhaie T, Masnavi MR (2014) Environmental design for ecological infrastructure of urban landscape through aggregate with outlier principle (AWOP) in order to enhance the quality of urban life; the case of district two, Tehran City. J Environ Stud 40(3):559–572. https://doi.org/10.22059/jes.2014.52205
Krikken F, Lehner F, Haustein K, Drobyshev I, Van Oldenborgh GJ (2021) Attribution of the role of climate change in the forest fires in Sweden 2018. Nat Hazards Earth Syst Sci 21(7):2169–2179. https://doi.org/10.5194/nhess-21-2169-2021
Kussul N, Fedorov O, Yailymov B, Pidgorodetska L, Kolos L, Yailymova H, Shelestov A (2023) Fire danger assessment using moderate-spatial resolution satellite data. Fire 6(2):72. https://doi.org/10.3390/fire6020072
Mansourihanis O, Tilaki MJM, Yousefian S, Zaroujtaghi A (2023) A computational geospatial approach to assessing land-use compatibility in urban planning. Land 12(11):2083. https://doi.org/10.3390/land12112083
Mansourihanis O, Tilaki MJM, Sheikhfarshi S, Mohseni F, Seyedebrahimi E (2024a) Addressing urban management challenges for sustainable development: analyzing the impact of neighborhood deprivation on crime distribution in Chicago. Societies 14(8):139. https://doi.org/10.3390/soc14080139
Mansourihanis O, Tilaki MJM, Kookhaei T, Zaroujtaghi A, Sheikhfarshi S, Abdoli N (2024b) Integrating geospatial intelligence and spatio-temporal modeling for monitoring tourism-related carbon emissions in the United States. Manage Environ Qual Int J. https://doi.org/10.1108/meq-04-2024-0156
Masaeli N, Afshari E, Baniasadi E, Baharlou-Houreh N, Ghaedamini M (2023) Experimental analysis of water transfer and thermal–hydraulic performance of membrane humidifiers with three flow field designs. Appl Energy 336:120823. https://doi.org/10.1016/j.apenergy.2023.120823
Masoodian SA, Keikhosravi kiany MS (2020) Trend analysis of snow accumulation season start in Iran using remote sensing data. Geogr Environ Plann 31(1):1–14. https://doi.org/10.22108/gep.2020.120775.1249

Matin MA, Chitale VS, Murthy MSR, Uddin K, Bajracharya B, Pradhan S (2017) Understanding forest fire patterns and risk in Nepal using remote sensing, geographic information system and historical fire data. Int J Wildland Fire 26(4):276. https://doi.org/10.1071/wf16056

Miller C, Ager AA (2013) A review of recent advances in risk analysis for wildfire management. Int J Wildland Fire 22(1):1. https://doi.org/10.1071/wf11114

Mishra M, Guria R, Baraj B, Nanda AP, Santos CaG, Da Silva RM, Laksono F (2024) a. T. Spatial analysis and machine learning prediction of forest fire susceptibility: a comprehensive approach for effective management and mitigation. The Science of the Total Environment 926:171713. https://doi.org/10.1016/j.scitotenv.2024.171713

Modarres R, Ghadami M, Naderi S, Naderi M (2018) Future heat stress arising from climate change on Iran's population health. Int J Biometeorol 62(7):1275–1281. https://doi.org/10.1007/s00484-018-1532-4

Mohimi A, Esmaeily A (2023) Spatiotemporal analysis of urban sprawl using a multi-technique approach and remote sensing satellite imagery from 1990 to 2020: Kerman/Iran. Environ Dev Sustain 26(7):18033–18068. https://doi.org/10.1007/s10668-023-03378-8

Morckel V, Durst N (2021) Using emerging hot spot analysis to explore spatiotemporal patterns of housing vacancy in Ohio metropolitan statistical areas. Urban Affairs Rev 59(1):309–328. https://doi.org/10.1177/10780874211065014

Moreno M, Bertolín C, Arlanzón D, Ortiz P, Ortiz R (2023) Climate change, large fires, and cultural landscapes in the mediterranean basin: an analysis in southern Spain. Heliyon 9(6):e16941. https://doi.org/10.1016/j.heliyon.2023.e16941

Moriondo M, Good P, Durao R, Bindi M, Giannakopoulos C, Corte-Real J (2006) Potential impact of climate change on fire risk in the mediterranean area. Climate Res 31:85–95. https://doi.org/10.3354/cr031085

Nasiri V, Heidarlou HB, Alchin AA, Moradi F, Rahmanian S, Afshari S, Maftei C, Griess VC (2023) How do conservation policies, climate and socioeconomic changes impact Hyrcanian forests of northern Iran? Ecological Informatics 78:102351. https://doi.org/10.1016/j.ecoinf.2023.102351

Nikolopoulos EI, Destro E, Bhuiyan MaE, Borga M, Anagnostou EN (2018) Evaluation of predictive models for post-fire debris flow occurrence in the western United States. Nat Hazards Earth Syst Sci 18(9):2331–2343. https://doi.org/10.5194/nhess-18-2331-2018

Noroozi J, Talebi A, Doostmohammadi M, Bagheri A (2020) The Zagros mountain range. In: Plant and vegetation, pp 185–214. https://doi.org/10.1007/978-3-030-45212-4_6

Papagiannaki K, Giannaros T, Lykoudis S, Kotroni V, Lagouvardos K (2020) Weather-related thresholds for wildfire danger in a mediterranean region: the case of Greece. Agric For Meteorol 291:108076. https://doi.org/10.1016/j.agrformet.2020.108076

Politi N, Vlachogiannis D, Sfetsos A, Gounaris N (2023) Fire weather assessment of future changes in fire weather conditions in the Attica Region. Environ Sci Proc 26(1):186. https://doi.org/10.3390/environsciproc2023026186

Pontius RG (2000) Quantification error versus location error in comparison of categorical maps. Photogrammetric Eng Remote Sens 66(8):1011–1016. https://dialnet.unirioja.es/servlet/articulo?codigo=708535

Preisler HK, Ager AA, Wisdom MJ (2005) Statistical methods for analysing responses of wildlife to human disturbance. J Appl Ecol 43(1):164–172. https://doi.org/10.1111/j.1365-2664.2005.01123.x

Rabiei-Dastjerdi H, McArdle G (2020) Identifying patterns of neighbourhood change based on spatiotemporal analysis of Airbnb data in Dublin. In Proceedings of the 2020 4th international conference on smart grid and smart cities (ICSGSC), Osaka, Japan. https://doi.org/10.1109/icsgsc50906.2020.9248558

Rädler AT, Groenemeijer PH, Faust E, Sausen R, Púčik T (2019) Frequency of severe thunderstorms across Europe expected to increase in the 21st century due to rising instability. NPJ Clim Atmospheric Sci 2(1). https://doi.org/10.1038/s41612-019-0083-7

Rajitha K, Mukherjee CK, Chandran RV, Mohan MMP (2010) Land-cover change dynamics and coastal aquaculture development: a case study in the East Godavari delta, Andhra Pradesh, India using multi-temporal satellite data. Int J Remote Sens 31(16):4423–4442. https://doi.org/10.1080/01431160903277456

Reddy CS, Unnikrishnan A, Bird NG, Faseela VS, Asra M, Manikandan TM, Rao PVN (2020) Characterizing vegetation fire dynamics in myanmar and South Asian countries. J Indian Soc Remote Sens 48(12):1829–1843. https://doi.org/10.1007/s12524-020-01205-5

Rodrigues M, González-Hidalgo JC, Peña-Angulo D, Jiménez-Ruano A (2018) Identifying wildfire-prone atmospheric circulation weather types on mainland Spain. Agric For Meteorol 264:92–103. https://doi.org/10.1016/j.agrformet.2018.10.005

Roshan G, Yousefi R, Fitchett JM (2015) Long-term trends in tourism climate index scores for 40 stations across Iran: the role of climate change and influence on tourism sustainability. Int J Biometeorol 60(1):33–52. https://doi.org/10.1007/s00484-015-1003-0

Roshan G, Ghanghermeh A, Grab SW (2023) Spatio-temporal changes in sunshine duration over Iran: impact of physical geographic components. Meteorol Atmos Phys 135(3). https://doi.org/10.1007/s00703-023-00959-0

Roshan G, Sarli R, Grab SW, Nasiri V, Socha J (2024a) Elevational trends of land surface temperature in the Alborz Mountains within the context of global warming. Stoch Env Res Risk Assess 38(5):1721–1739. https://doi.org/10.1007/s00477-023-02651-6

Roshan G, Sarli R, Ghanghermeh A, Taherizadeh M, Niknam A (2024b) Using satellite-derived land surface temperatures to clarify the spatiotemporal warming trends of the Alborz Mountains in northern Iran. J Mt Sci 21(2):449–469. https://doi.org/10.1007/s11629-023-8384-z

Rustowska B (2022) Long-term wildfire effect on nutrient distribution in silver birch (<i>Betula pendula Roth) biomass. Soil Sci Annual 73(2):1–14. https://doi.org/10.37501/soilsa/149943

Sadrianzadeh M, Kharazi HG, Eslami H, Fathian H, Telvari A (2023) Impact of climate change on the precipitation trend and phase in snow-dominated mountain basins (Central Zagros Mountains, Iran). Water Resour 50(1):48–57. https://doi.org/10.1134/s0097807823010141

Salehi Mava F, Khatami SM, Ranjbar E (2022) An analysis on the factors affecting the creation of event-oriented urban public spaces case study: central part of Tehran (District 12). Monthly Sci J Bagh-e Nazar 19(106):85–98. https://doi.org/10.22034/bagh.2021.269717.4780

Schunk C, Wastl C, Leuchner M, Menzel A (2016) Fine fuel moisture for site- and species-specific fire danger assessment in comparison to fire danger indices. Agric For Meteorol 234–235. https://doi.org/10.1016/j.agrformet.2016.12.007

Semenova I, Sumak K (2022) Dynamics of fire weather conditions in the mixed forest areas of Belarus and Ukraine under recent climate change. Geofizika 39(1):71–83. https://doi.org/10.15233/gfz.2022.39.10

Soualah L, Bouzekri A, Chenchouni H (2024) Hoping the best, expecting the worst: forecasting forest fire risk in Algeria using fuzzy logic and GIS. Trees Forests People 17:100614. https://doi.org/10.1016/j.tfp.2024.100614

Sousa-Silva R, Verbist B, Lomba Â, Valent P, Suškevičs M, Picard O, Hoogstra-Klein MA, Cosofret V, Bouriaud L, Ponette Q, Verheyen K, Muys B (2018) Adapting forest management to climate change in Europe: linking perceptions to adaptive responses. For Policy Econ 90:22–30. https://doi.org/10.1016/j.forpol.2018.01.004

Tian Y, Wu Z, Li M, Wang B, Zhang X (2022) Forest fire spread monitoring and vegetation dynamics detection based on multi-source remote sensing images. Remote Sens 14(18):4431. https://doi.org/10.3390/rs14184431

Tremblay JA, Boulanger Y, Cyr D, Taylor AR, Price DT, St-Laurent M (2018) Harvesting interacts with climate change to affect future habitat quality of a focal species in eastern Canada's boreal forest. PLoS ONE 13(2):e0191645. https://doi.org/10.1371/journal.pone.0191645

Vadrevu KP (2021) Fire danger indices and methods: an appraisal. In: CRC Press eBooks, pp. 201–232. https://doi.org/10.1201/9780429022258-12

Varela V, Vlachogiannis D, Sfetsos A, Karozis S, Politi N, Giroud F (2019) Projection of forest fire danger due to climate change in the French Mediterranean Region. Sustainability 11(16):4284. https://doi.org/10.3390/su11164284

Vigna I, Battisti L, Ascoli D, Besana A, Pezzoli A, Comino E (2023) Integrating cultural ecosystem services in wildfire risk assessment. Landsc Urban Plann 243:104977. https://doi.org/10.1016/j.landurbplan.2023.104977

Zafarani H, Soghrat M (2012) Simulation of ground motion in the Zagros region of Iran using the specific barrier model and the stochastic method. Bull Seismol Soc Am 102(5):2031–2045. https://doi.org/10.1785/0120110315

Publisher's note Springer Nature remains neutral with regard to jurisdictional claims in published maps and institutional affiliations.

Springer Nature or its licensor (e.g. a society or other partner) holds exclusive rights to this article under a publishing agreement with the author(s) or other rightsholder(s); author self-archiving of the accepted manuscript version of this article is solely governed by the terms of such publishing agreement and applicable law.